AGU PUBLICATIONS

Geochemistry, Geophysics, Geosystems

RESEARCH ARTICLE
10.1002/2015GC005869

Special Section:
Oceanic detachment faults

Geologic evolution of the Lost City Hydrothermal Field

Alden R. Denny[1,2], Deborah S. Kelley[1], and Gretchen L. Früh-Green[3]

[1]School of Oceanography, University of Washington, Seattle, Washington, USA, [2]Now at Centre for Geobiology, University of Bergen, Bergen, Norway, [3]Department of Earth Sciences, ETH-Zurich, Zurich, Switzerland

Key Points:
- The Lost City Hydrothermal Field is more complex and extensive than previously thought
- Unexplored extinct fields are downslope and to the west from the active field

Correspondence to:
A. R. Denny,
Alden.Denny@geo.uib.no

Citation:
Denny, A. R., D. S. Kelley, and G. L. Früh-Green (2015), Geologic evolution of the Lost City Hydrothermal Field, *Geochem. Geophys. Geosyst.*, *17*, 375–394, doi:10.1002/2015GC005869.

Received 23 APR 2015
Accepted 4 DEC 2015
Accepted article online 14 DEC 2015
Published online 11 FEB 2016

Abstract The Lost City Hydrothermal Field (LCHF) is a novel serpentinite-hosted vent field located on the Atlantis Massif southern wall. Results of 2 m resolution bathymetry, side scan, and video and still imagery, integrated with direct submersible observations provide the first high-resolution geologic map of the LCHF. These data form the foundation for an evolutionary model for the vent system over the past >120,000 years. The field is located on a down-dropped bench 70 m below the summit of the massif. The bench is capped by breccia and pelagic carbonate deposits underlain by variably deformed and altered serpentinite and gabbroic rocks. Hydrothermal activity is focused at the 60 m tall, 100 m across, massive carbonate edifice "Poseidon," which is venting 91°C fluid. Hydrothermal activity declines south and west of the Poseidon complex and dies off completely at distances greater than 200 m. East of Poseidon, the most recent stage of hydrothermal flow is characterized by egress of diffuse fluids from narrow fissures within a low-angle, anastomosing mylonite zone. South of the area of current hydrothermal activity, there is evidence of two discrete previously unrecognized relict fields. Active venting sites defined by carbonate-filled fissures that cut the carbonate cap rock at the summit of the massif mark the present-day northernmost extent of venting. These spatial relationships reflect multiple stages of field development, the northward migration of venting over time, and the likely development of a nascent field at the massif summit.

1. Introduction

Oceanic core complexes (OCCs) are ubiquitous features of ultraslow and slow spreading environments [*Cannat et al.*, 1997; *Blackman et al.*, 2002; *Karson et al.*, 2006; *Smith et al.*, 2006, 2008; *Escartín et al.*, 2008; *Petersen et al.*, 2009; *Pedersen et al.*, 2010]. Their formation is fundamental to the development of slow spread oceanic crust and in the generation of both black smoker and Lost City-type hydrothermal systems [e.g., *Kelley et al.*, 2001, 2005, 2015; *Charlou et al.*, 2002; *McCaig et al.*, 2007; *Escartín et al.*, 2008; *Petersen et al.*, 2009; *Pedersen et al.*, 2010]. Oceanic core complexes, formed by asymmetric exhumation along long-lived, spreading-parallel normal faults, commonly expose serpentinized mantle peridotite and variably altered and deformed gabbros. [*Cannat et al.*, 1997; *Karson et al.*, 2006; *Smith et al.*, 2006]. These structures share similarities with terrestrial metamorphic core complexes [*Howard et al.*, 1987; *Dick*, 1989; *Karson*, 1990; *Mutter and Karson*, 1992; *Tucholke et al.*, 1998; *Blackman et al.*, 2002; *Reston et al.*, 2002; *John and Cheadle*, 2010].

Formation of OCCs is considered to be controlled predominantly by magmatic intrusion rates. Core complexes are interpreted to initiate during periods of low magmatic input along ultraslow and slow spreading ridges [*Tucholke et al.*, 1998; *Escartín et al.*, 2008; *MacLeod et al.*, 2009]. This likely contributes to their prevalence at ridge-transform intersections and at nontransform offsets. Core complexes are thought to initiate as deep-rooted high-angle normal faults on the ridge axis, which roll-over to a low-angle fault due to flexural unloading [*Buck*, 1988; *Tucholke et al.*, 1998; *deMartin et al.*, 2007; *Morris et al.*, 2009; *Macleod et al.*, 2011]. The rise-height of magmatic intrusion above or below the brittle-ductile transition zone controls the relative proportions of exhumed peridotite versus gabbroic rocks [*Olive et al.*, 2010]. Faulting on OCCs lasts for several million years, with asymmetric spreading either jumping ridgeward to a new fault, or shifting to magmatic spreading if the magma supply increases [*Blackman et al.*, 2002; *Buck et al.*, 2005; *MacLeod et al.*, 2009]. The surfaces of OCCs are typically characterized by spreading-parallel corrugations along broadly curved low-angle surfaces that are interpreted to be long-lived extensional faults [*Cann et al.*, 1997; *Tucholke et al.*, 1998; *Escartín and Cannat*, 1999; *Reston et al.*, 2002; *Blackman et al.*, 2002; *Searle et al.*, 2003; *Karson et al.*, 2006; *Smith et al.*, 2008].

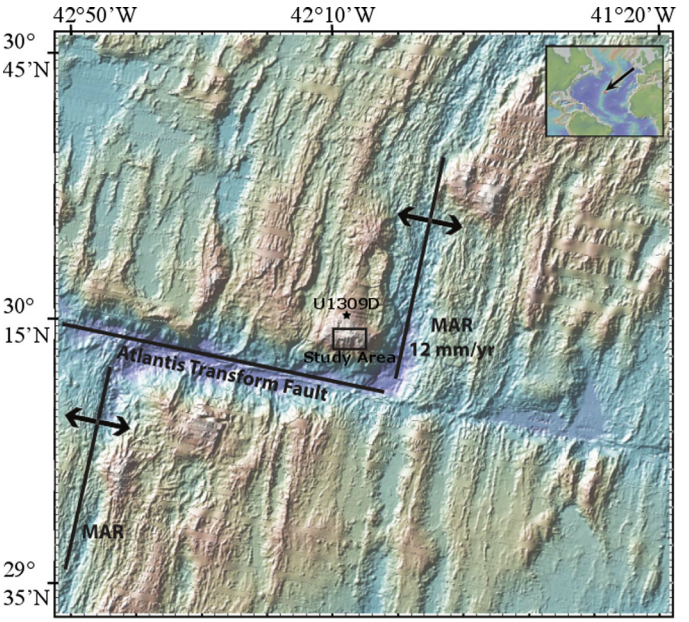

Figure 1. Location map for the Atlantis Massif, located at 30°N between the Atlantis Transform Fault and the Mid-Atlantic Ridge. The study area is at the summit of the massif at a water depth of 740 m. IODP drill site U1309D is labeled on the map with a star. This map is viewed in a WGS-1984 geographic datum with a global Mercator projection, and created using the GeoMapApp tool [*Ryan et al*., 2009].

The Atlantis Massif is a well-mapped and studied OCC at 30°N on the inside corner high between the Atlantis Transform Fault and the Mid-Atlantic Ridge [*Blackman et al*., 2002; *Kelley et al*., 2002; *Karson et al*., 2006; *Blackman et al*., 2008, 2009; *Kelley and Shank*, 2010] (Figure 1). The summit of the central dome of the massif was drilled during IODP Expeditions 304/305 [*Blackman et al*., 2011; *Schroeder and John*, 2004]. Early bathymetric studies of the Atlantis Massif showed that it was a type location for research on OCCs, exhibiting the hallmark spreading-parallel corrugations, and a distinct fault at the footwall-hanging wall contact [*Cann et al*., 1997; *Blackman et al*., 2002].

In 2000, during a survey with the *Argo* towed camera, the novel Lost City Hydrothermal Field (LCHF) was discovered [*Kelley et al*., 2001]. The field hosts spectacular carbonate towers rising 60 m above the seafloor that vent basic fluids enriched in hydrogen, methane, and other low molecular weight hydrocarbons [*Kelley et al*., 2001, 2005; *Proskurowski et al*., 2008; *Lang et al*., 2010]. Since that initial discovery, the importance of OCC's in formation of both black smoker and alkaline, Lost City-type systems has attracted great interest, in part because of the novel microbial life that inhabits the chimneys [*Schrenk et al*., 2003; *Brazelton et al*., 2006, 2010], but also for researchers interested in exploration for life on other planets [*Kelley et al*., 2005; *Schulte et al*., 2006; *Schrenk et al*., 2013; *McCollom and Seewald*, 2013; *Hsu et al*., 2015]. Much of this interest stems from the growing recognition of serpentinization reactions and their importance for abiogenic synthesis of hydrocarbons [*Holm and Charlou*, 2001; *Kelley et al*., 2001, 2005; *McCollom and Seewald*, 2006; *Proskurowski et al*., 2006; *McCollom and Bach*, 2009; *Lang et al*., 2010, 2012] and perhaps to the origin of life itself [*Martin et al*., 2008; *Holm*, 2012]. This paper presents the first detailed geologic description of the LCHF based on meter-scale resolution bathymetry maps derived from data collected with the AUV *ABE* (Figure 2), the Deep-Towed DSL-120 side-scan sonar, and direct observations from DSV *Alvin* and the ROV *Hercules*. In concert, these data are used to synthesize an evolutionary history of the Lost City system, including an estimate of the maximum field extent and venting duration.

2. Methods

Submersible and remotely operated vehicle data were compiled from expeditions funded by the National Science Foundation aboard the *R/V Atlantis* (cruise AT3-60 in 2000 and AT7-34 in 2003) and a NOAA-supported effort aboard the *R/V Brown* in 2005 (Figure 3). Cruise AT3-60 conducted high-resolution DSL-120 side scan surveys of the central and southern portion of the Atlantis Massif, including the southern scarp and the LCHF (Figure 4, bottom), and dredges from the southern fault slope and massif summit [*Blackman et al*., 2002]. Digital still imagery was collected with the towed vehicle *Argo*, from which the field was discovered in 2000 [*Kelley et al*., 2001]. Limited video, still imagery, and samples from the LCHF were collected on the first dive to the field (DSV *Alvin* dive 3651). During the AT7-34 return cruise to Lost City in 2003, 19 dives were completed with the DSV *Alvin* (Figure 3) and eight missions were undertaken with the AUV *ABE* [*Kelley et al*., 2005; *Karson et al*., 2006]. The *Alvin* dives collected extensive video and still imagery covering a 2 km section to a depth of 1200 m to the south of the LCHF (Figure 3). During the AT7-34 expedition, *Alvin* collected 40 well-located samples of carbonate chimney and fissure deposits and 69 samples of basement rock. The *ABE* missions acquired

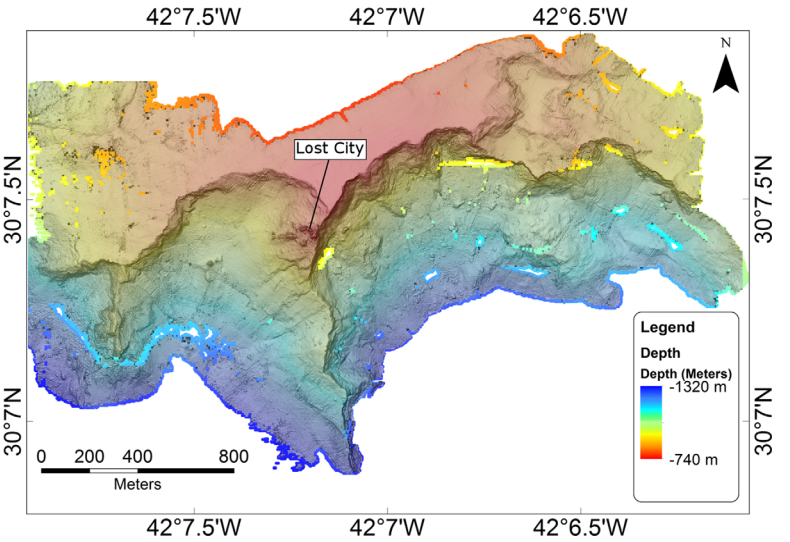

Figure 2. AUV *ABE* bathymetry of the Atlantis Massif summit gridded to 2 m horizontal resolution. All AUV maps are displayed in the WGS-1984 datum with a local planar Mercator projection. These data are available through the Marine Geoscience Data System hosted at Lamont-Doherty Earth Observatory as part of IEDA [*Kelley et al.*, 2015]

high-resolution multibeam bathymetry [*Kelley et al.*, 2001, 2005; *Karson et al.*, 2006]. In 2005, the R/V *Brown* hosting the ROV *Hercules* and *Medea* system visited the LCHF for 9 days as part of a NOAA Ocean Exploration program in collaboration with the University of Washington and the Institute for Exploration at the University of Rhode Island. The 2005 program collected high-definition video and still imagery of the field and limited rock samples. Hydrothermal carbonate structures are delineated by names given to them by the science teams during the 2000, 2003, and 2005 field campaigns.

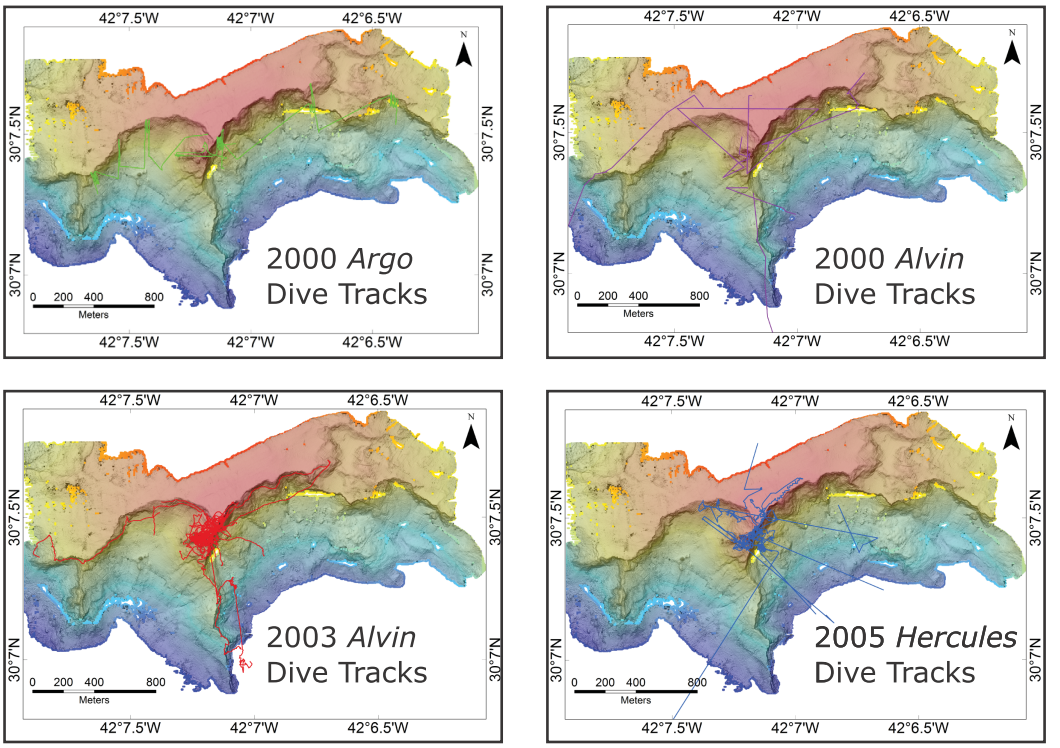

Figure 3. AUV *ABE* 2 m resolution bathymetry overlain with submersible dive tracklines illustrating the direct video and still image coverage used in this study. From upper left: 2000 Argo towed camera vehicle, 2000 Alvin HOV, 2003 Alvin HOV, and 2005 Hercules ROV.

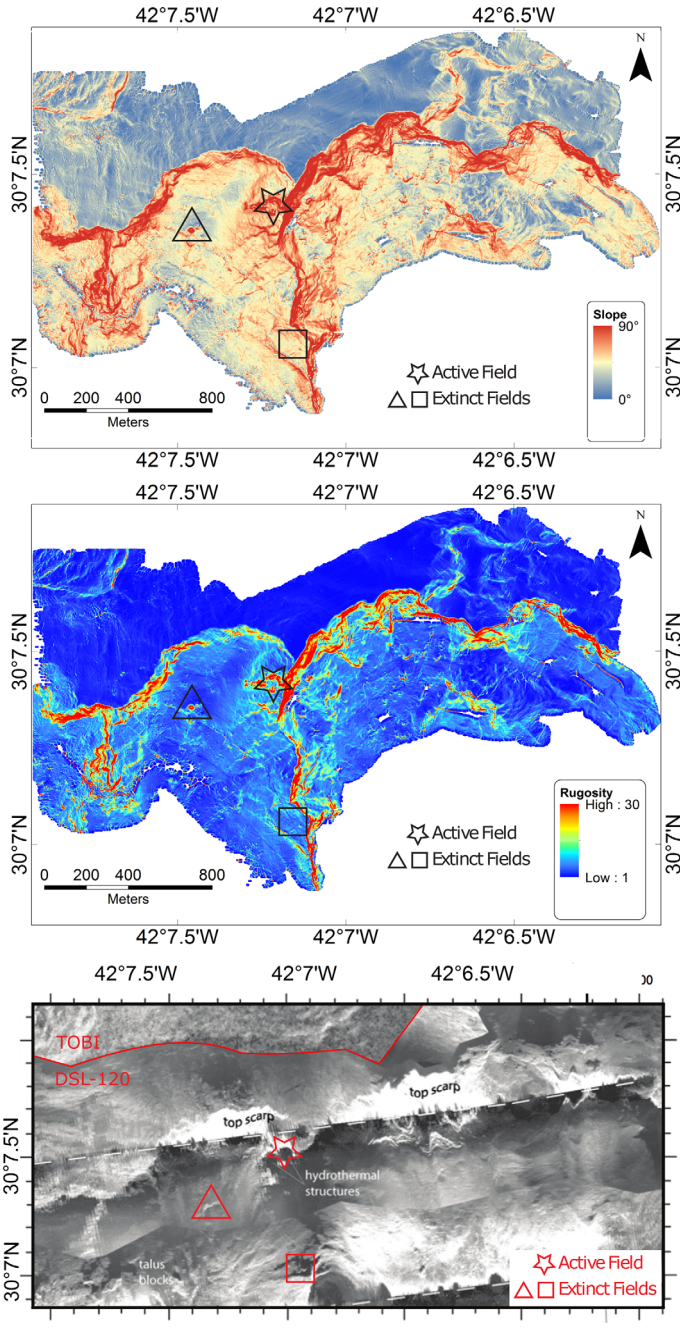

Figure 4. (top) Slope map derived from 2 m resolution bathymetry collected by the AUV *ABE* and processed in ArcGIS. Values in red denote steep slopes, blue delineate more gentile slopes. (middle) Rugosity map derived from 2 m resolution bathymetry collected by the AUV *ABE* and processed with the GMET ArcGIS extension [*Roberts et al.*, 2010]. Warmer colors delineate rougher rugosity, cooler more smooth rugosity values. (bottom) DSL-120 side-scan sonar imagery crossing the summit of the Atlantis Massif (adapted from *Blackman et al.* [2002]). The sidescan images are overlain on coarse-scale TOBI sidescan data. The sidescan data clearly show the main Poseidon edifice in the core of the Lost City Hydrothermal Field, as well as the surrounding active and inactive carbonate towers. DSL-120 Sidescan was navigated by layback position. The DSL-120 data are available through the Marine Geoscience Data System [*Blackman et al.*, 2015].

2.1. Navigation

The AUV *ABE* and DSV *Alvin* were navigated using an onboard doppler velocity sensor (DVL) and a long baseline (LBL) transponder net to insure high accuracy in positioning of vehicles and resultant bathymetry, video transects, and samples. Postcruise, the track lines were renavigated using NavProc with procedures established by *Ferrini et al.* [2004] to integrate DVL and LBL navigation for best fit of locations. Directly adjacent to the core of the LCHF, the navigation is accurate to ±4 m; away from the transponder array, offsets increased to ±10 m for *Alvin* navigation. The navigation errors were due to uncertainty in the position of the transponders within their tether watch circle.

The 2005 dive program did not use an LBL net, resulting in comparatively poor dive navigation. Consequently, video imagery was predominantly used to locate the ROV *Hercules* in proximity to previously located features. Because of the superior navigation during the 2003 dive program, unit positions from 2000 and 2005 dives were relocated based on landmarks fixed during 2003. In addition to geomorphological interpretations based on the *ABE* bathymetry, all of the 2000 and 2003 *Alvin* and 2005 *Hercules* video and still imagery were utilized to locate geologic contacts.

2.2. Bathymetry

During 17 missions, *ABE* collected 3.3 km^2 of bathymetry across the southern wall of the Atlantis Massif directly adjacent to the LCHF and southern summit of the massif using SM2000 multibeam sonar (Figure 2). The SM2000 multibeam sonar on *ABE* was positioned in both a down-looking and side-looking orientation to best image the near-vertical cliffs and hydrothermal spires on the southern summit of the Atlantis Massif

[*Karson et al*., 2006]. Bathymetric data were compiled in MBSystem [*Caress and Chayes*, 2014] and gridded in Fledermaus to 2 × 2 m resolution. All bathymetry, dive tracks, and sample/transponder locations were collated in ArcGIS, including derived products of slope (Figure 4, top) and rugosity (Figure 4, middle) created with the MGET ArcGIS extension [*Roberts et al*., 2010]. Rugosity is a measure of the topographic roughness based on the average difference in elevation of a reference cell to its eight adjoining cells. In this study, rugosity was used to establish the locations of boulder fields and other geomorphologic features.

2.3. Mapping of Units

Geologic unit and fault contacts were established based on samples collected during dive missions correlated to both dive video and down-looking still images. In concert, these data were used to define the outcrop morphology of various units. Each contact was first delineated directly from the navigated location of the submersible, and then corrected for position based on the vehicle depth. At distances in excess of 500 m from the LBL grid, vehicle depth provided the best N-S positional constraint. Lastly, mapped locations of unit contacts were connected by geomorphological characteristics, to create as best as possible, an outcrop-scale interpretation of both basement rock and hydrothermal units. The varying levels of certainty are noted in the geologic map by the line weight used and annotated in the legend. Solid lines denote areas of direct observation and sampling. A dashed line is used where sampling or observation is sparse but the geomorphologic indicators are reasonably clear. A dashed line with "?" is used where there is a high level of uncertainty regarding the unit boundaries and composition.

3. Background Geology

3.1. Atlantis Massif

The southern exposure of the Atlantis Massif rises 3800 m from the base of the Atlantis Transform Fault, culminating in a shear cliff face ~200 m high. This cliff rises to a depth of 740 mbsl (meters below sea level). It is deeply embayed due to mass wasting and faulting, which exposes massive serpentinite with lesser gabbroic rocks. The wall terminates in a 50–100 m thick variably deformed zone that defines the main Atlantis Massif Detachment Shear Zone (DSZ) at the summit of the massif (Figures 5a–5c) [*Kelley et al*., 2005; *Karson et al*., 2006]. Five kilometers north of the LCHF, the Integrated Ocean Drilling Program (IODP) drilled Hole U1309D into >1400 m of gabbro, with rare talc bodies [*Expedition Scientific Party*, 2005] (Figure 1, star). Stratigraphic, petrologic, and geochemical analyses were consistent with variable melt intrusion along the Mid-Atlantic Ridge axis in this area.

The central dome and southern ridge of the Atlantis Massif differ strongly in the exposure extent of ultramafic material [*Blackman et al*., 2011]. A model proposed by *Ildefonse et al*. [2007] introduces the possibility that the ultramafic material on the southern ridge is in fact a sheath of highly deformed rock surrounding large intrusive bodies. In this model, the southern wall is simply a region of anomalously deep intrusion of gabbroic bodies, which caused the exhumation of a large body of ultramafic material only at this location. Although this model provides both a proposed heat source for the LCHF and continuity with the IODP 304-305 expedition coring results, it is not well substantiated by the LCHF fluid chemistry (high pH, absence of both metals, and carbon dioxide). Warm peridotite rocks at depth may provide sufficient heat to drive fluid flow at this site [*Proskurowski et al*., 2006, 2008].

3.2. Gabbro

Variably deformed and altered gabbro lenses and isolated gabbroic bodies comprise <30% of the outcrop exposure of the southern wall [*Karson et al*., 2006]. This is in sharp contrast to results from IODP Expeditions 304/305 in which the core was dominated by gabbroic lithologies that lacked extensive ductile deformation fabrics [*Ildefonse et al*., 2007]. Gabbroic lithologies collected at the southern wall include medium to coarse-grained olivine gabbros with less abundant gabbro, gabbronorites, rare highly evolved oxide gabbros, and local rodingites [*Boschi et al*., 2006; *Schroeder and John*, 2004]. The gabbros are dominated by primary plagioclase and clinopyroxene, with minor oxide minerals, orthopyroxene, and olivine. Samples collected along the eastern area of the southern wall provide evidence for multiple intrusions and melt-rock interaction.

The gabbroic rocks were impacted by multiple stages of alteration and deformation during uplift and cooling (Figure 5). Granulite-facies mineral assemblages and deformation fabrics were overprinted by amphibolite-facies assemblages during the early phases of exhumation [*Schroeder and John*, 2004;

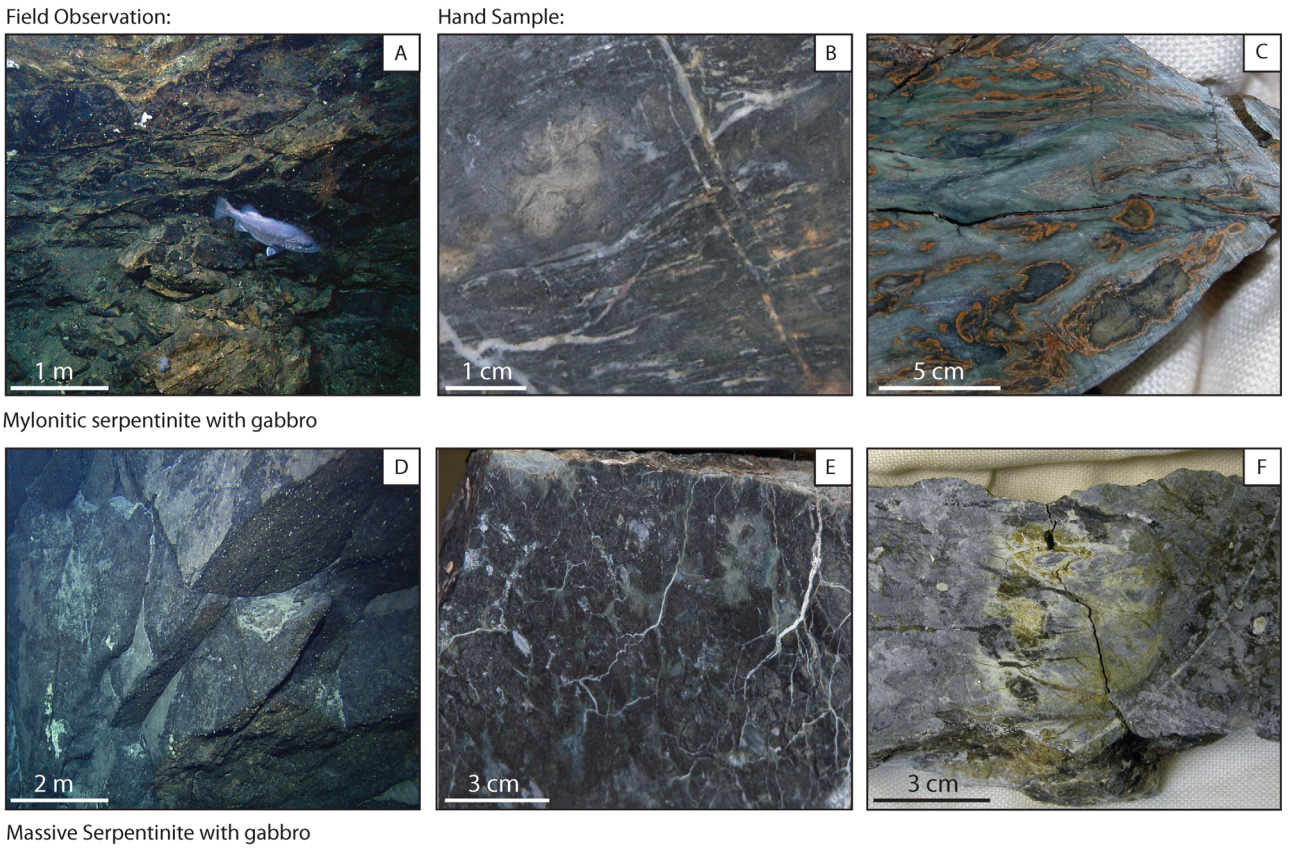

Figure 5. Coregistered outcrop and hand-sample images of serpentinite rock units on the southern face of the Atlantis Massif. (a) Mylonitic serpentinite in outcrop with well-defined subhorizontal, anatomosing shear zones lacking blocky fracture (image from the *ROV Hercules*). (b) Hand-sample image of augen and focused mylonitic shear zones. (c) Hand-sample image of talc-tremolite mylonite. (d) Massive serpentinite in outcrop with large blocky fracture and no pervasive shear fabric (image from the *DSV Alvin*). (e) Hand sample of serpentinite with static alteration textures, patches of metasomatic talc-amphibole domains, and calcite veining. (f) Hand sample of statically altered gabbroic protolith with metasomatically altered serpentinite domains. All outcrop image locations are shown in Figure 9b.

Boschi et al., 2006]. This high-temperature deformation is locally focused and results in mylonitic to ultramylonitic textures. Petrographic and textural relationships indicate that high-temperature deformation occurred during the initial faulting at depth below the ridge axis. The high-grade assemblages are overprinted by greenschist-facies assemblages marked by tremolite-actinolite amphiboles ± chlorite [*Schroeder and John*, 2004; *Boschi et al*., 2006]. This stage of alteration is interpreted by *Schroeder and John* [2004] to be due to unroofing of the core complex and fluid flow within the Detachment Shear Zone.

3.3. Serpentinized Peridotite

Variably altered and deformed serpentinized harzburgite comprises >70% of the exposed rock along the southern wall [*Karson et al*., 2006; *Boschi et al*., 2006]. The ultramafic protolith is dominantly a spinel harzburgite with medium to coarse-grained porphyroclastic texture [*Boschi et al*., 2006]. Alteration in the samples collected is pervasive, with all samples showing >70% alteration to serpentinite. However, massive and steep outcrops stratigraphically lower and outside of the DSZ may represent less altered ultramafic rocks [*Blackman et al*., 2002]. The lack of fractures in these outcrops prevented sampling (Figures 5d–5f).

The serpentine mineral assemblage at all stages of alteration is fairly consistent, with lizardite ± chrysotile and trace antigorite present in pre, syn, and postmetasomatic textures [*Boschi et al*., 2006]. This constrains the temperature of formation to >425°C [*O'Hanley*, 1996; *Früh-Green et al*., 2003]. Brucite has not been detected in samples collected to date. Talc is present as a minor high-temperature alteration mineral in the peridoties and is a greenschist-facies mineral in the gabbroic rocks. In the peridotites, talc is an alteration product of orthopyroxene. It commonly occurs with tremolite and/or chlorite in low-temperature (<∼400°C) metasomatic zones in the serpentinites [*Boschi et al*., 2006]. Talc overprinting is both synkinematic and postkinematic, with talc acting as a strain localizing mineral because of its low shear strength

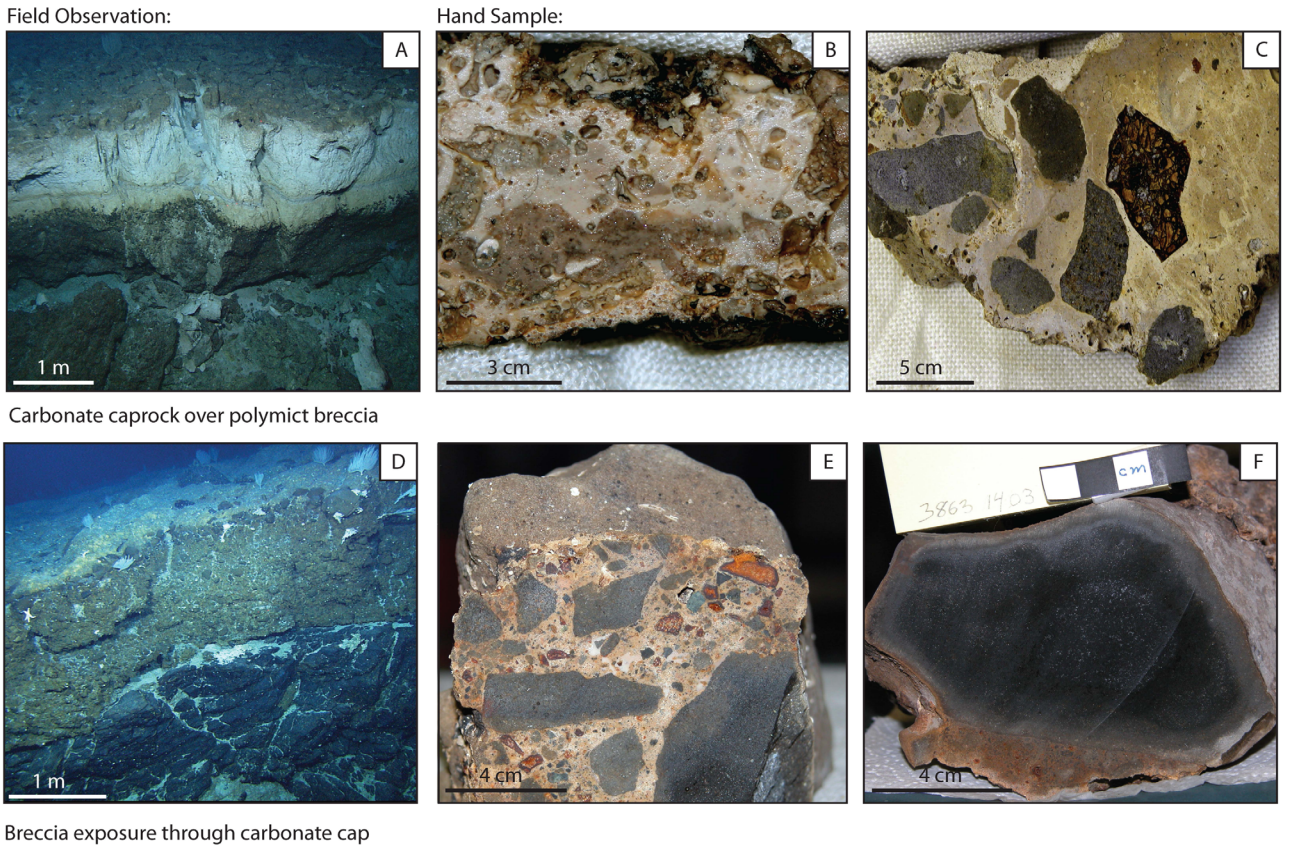

Figure 6. Coregistered outcrop and hand-sample images of polymict breccia and pelagic carbonate cap from the southern summit of the Atlantis Massif. (a) Outcrop image of mylonitic serpentinite zone uncomformably overlain by a polymict breccia and pelagic carbonate caprock (image from the *ROV Hercules*). (b) Hand-sample image of carbonate caprock with benthic invertebrate inclusions. (c) Hand-sample image of polymict breccia grading into pelagic carbonate sampled proximal to the contact with the underlying breccia with matrix-supported clasts of basalt and serpentinite. (d) Outcrop image of mylonitic serpentinite with overlying polymict breccia, note the absence of an extensive carbonate caprock in this exposure (image from the *DSV Alvin*). (e) Hand sample of matrix-supported breccia with clasts of basalt, serpentinite, and metagabbro. (f) Hand sample of large basaltic clast with manganese crust found on top of a summit breccia exposure. All outcrop image locations are shown in Figure 9b.

[*Schroeder and John*, 2004]. Textural interpretation of the alteration sequence indicates a consistent overprinting of lower temperature phases on higher-temperature minerals [*Schroeder et al*., 2002; *Früh-Green et al*., 2003; *Boschi et al*., 2006]. A progression of decreasing temperature with increasing brittle deformation and localization within the detachment fault is highly characteristic of OCC's [*Buck et al*., 2005].

3.4. Detachment Shear Zone (DSZ)

The DSZ is composed of anastomosing zones of intense, focused deformation that forms mylonitic rocks, which enclose lenses of less deformed serpentinite and gabbro [*Karson et al*., 2006; *Boschi et al*., 2006]. Ribbon serpentine + talc ± tremolite commonly defines high strain deformation fabric, with primary serpentinite textures found only in lenses (Figures 5b and 5c) [*Schroeder et al*., 2002; *Boschi et al*., 2006; *Karson et al*., 2006; *Delacour et al*., 2008]. Within the DSZ, alteration of the harzburgite and gabbro protoliths is pervasive. Here metasomatic rocks with varying proportions of talc, Ca-rich amphibole, and chlorite are common; in some cases, only REE and Sr/Nd isotope ratios provide an unambiguous indication of the protolith material [*Boschi et al*., 2006; *Delacour et al*., 2008]. The greenschist-facies mineral assemblages are overprinted by lower-temperature phases with a distinct partitioning of talc-tremolite products into locally ultramylonitic lenses. Regions of focused intense deformation are more common in the talc-tremolite dominated zones. The mylonitic fabric dips gently to the west [*Karson et al*., 2006] and is highly variable through the upper 50–100 m of the massif's southern exposure.

3.5. Cap Rock

A polymict breccia and carbonate caprock lie unconformably over the summit of the Atlantis Massif (Figure 6) [*Kelley et al*., 2001; *Früh-Green et al*., 2003; *Karson et al*., 2006]. The breccia is up to ~1 m thick and composed

of variably rounded clasts of serpentinite, gabbro, talc-tremolite nodules, and subangular weathered basalt in a micritic carbonate matrix. The micritic carbonate matrix weathers to a characteristic reddish brown color on outcrop exposures. The unconformable contact between faulted mylonitic serpentinite and the overlying breccia indicates that breccia formation postdates detachment faulting [*Karson et al*., 2006].

A pelagic carbonate cap forms a well-lithified, 1–2 m thick, nearly horizontal deposit on the summit of the massif. It includes pelagic fossil-rich micritic carbonate and hydrothermal carbonate resulting from diffuse flow [*Früh-Green et al*., 2003; *Ludwig et al*., 2011] (Figures 6a–6c). The pelagic carbonate layer caps the southern summit of the Atlantis Massif and acts as a barrier to underlying hydrothermal flow, except in regions where the caprock is fractured. Based on C^{14} data, the cap rock age is at least 34 kyr [*Früh-Green et al*., 2003]; more recent analyses utilizing ^{230}Th techniques indicate an age of 93 kyr [*Ludwig et al*., 2011]. The cap rock is discontinuous across the summit: to the west of the summit, there are significant exposures of breccia with little to no pelagic carbonate (Figure 6d).

3.6. Hydrothermal Chimney Morphology

Chimney morphologies across the entire LCHF are highly variable, which in part reflect their evolutionary stage [*Kelley et al*., 2005; *Ludwig et al*., 2006]. Four stages of carbonate deposit evolution were defined by *Ludwig et al*. [2006], for the Lost City structures. Stage I is the direct egress of high pH fluid from serpentinized peridotite. This stage is exemplified in the far northeast portion of the field by nascent carbonate structures that grow directly on and out of a steep face of serpentinite bedrock (Figures 7a, 7b, 8e, and 8f). All Stage I structures are $<$1 m tall and composed of aragonite and brucite that typically show filamentous-like growth structures with high porosity. Their location is heavily controlled by foliations in the mylonitic serpentinite. Stage II results in the formation of delicate snow-white, highly friable carbonate towers, and flanges composed of aragonite and brucite (Figures 7c, 7d, 8a, and 8b). These precipitate from variable mixing of 40–90°C hydrothermal fluids and seawater. Progressive hydrothermal flow and mixing within the deposits fills in the highly porous deposits, providing cohesiveness to the edifices. Mature Stage III structures host distinct channels, are well lithified, and show progressive alteration of aragonite to calcite. Stage III structures reach up to 60 m in height. They are dominantly light to deep ivory in color depending on the age of the carbonate (carbonate progressively darkens in color with age at LCHF) (Figures 8a and 8b). The final Stage IV/V structures are progressively more lithified and less porous. Aragonite is completely replaced by calcite, and brucite is removed entirely through dissolution (Figures 7e and 7f). These structures are rounded, colonized by epifaunal populations; the oldest structures are dark brown. In the largest edifices, multiple growth stages are commonly present, consistent with their complex evolutionary histories.

4. Results

Detailed analysis of the bathymetry, dive video and still images, and recovered samples yield new geological interpretations and an evolutionary model of the LCHF and the Atlantis Massif summit. This investigation also resulted in the discovery of previously unreported proximal and distal extinct fields. Results from this study allow previous work at the LCHF to be placed in the broader evolutionary context. The following interpretations are based on direct submersible observation, and derived sonar products.

4.1. Faults

High-angle normal faults control the morphology of the south face of the Atlantis Massif, resulting in the formation of 800 m across embayments bounded by steep ridges (such as the one that hosts the LCHF). The embayments offset the OCC surface to the north up to 200 m and are constrained by the north-south trending high-angle normal faults (Figures 9a and 9b). The high-angle faults intersect and cut the basement rocks, and focus slope instability on the southern extent of the Atlantis Massif summit. There are two generations of high-angle normal faults expressed on the southern massif summit. One set of faults is oriented north-south. These faults have offsets of 10–20 m and extend $>$2 km south of the Atlantis Massif summit forming steep ridges that terminate at the Atlantis Transform Fault (Figure 9a). These faults control hydrothermal flow [*Kelley et al*., 2005; *Karson et al*., 2006; *Ludwig et al*., 2006] and show a sinusoidal expression due to recent mass wasting. The second set of faults has a smaller surficial expression. They mostly occur within, and just below the DSZ. They trend northwest-southeast and show far more variation in trend than the larger, north-south faults. These faults offset the basement rock by $<$10 m and are mainly evident by the relative thickness of the DSZ. Downslope and to the south, the expression of both types of normal faults

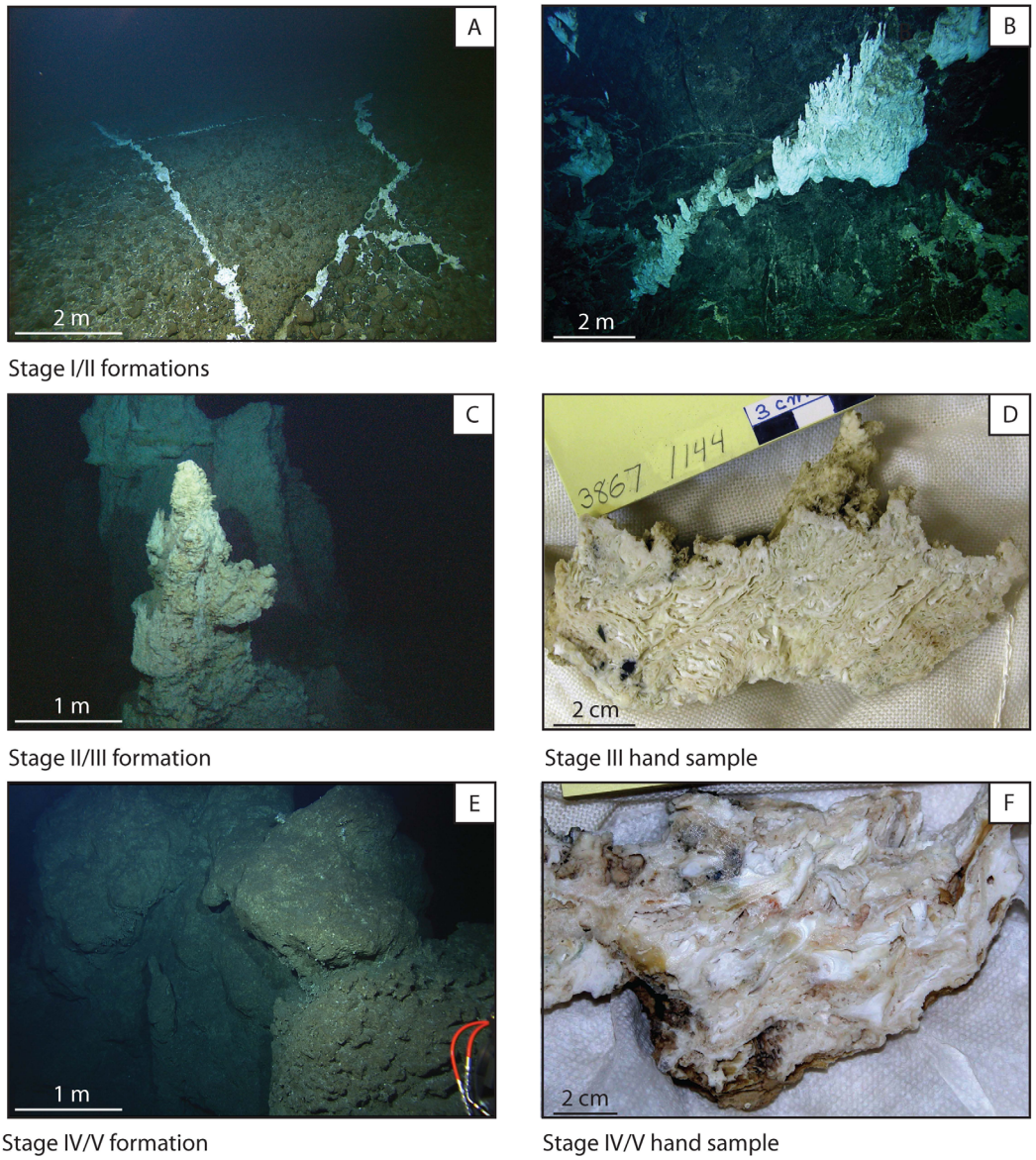

Figure 7. Examples of hydrothermal carbonate at the LCHF. Outcrop example of nascent venting (a) on the summit of the Atlantis Massif immediately to the north of LCHF and (b) on exposed serpentinite to the northeast of the LCHF. (c) Carbonate tower on razorback ridge running north from the central Poseidon complex and (d) accompanying hand sample of Stage II/III carbonate. (e) Well-rounded and indurated carbonate towers to the south of the Poseidon complex. The heavily indurated towers were not directly sampled due to their shape and robustness that prevented obtaining "handholds" with manipulators on the vehicles. (f) Hand sample of Stage IV/V carbonate collected from detrital slopes (shown in Figure 12). All seafloor images were taken with the *ROV Hercules*. All outcrop image locations are shown in Figure 9b.

is concealed by rubble and debris, obscuring the total fault throw. None of the high-angle normal faults interact with the breccia or carbonate caprock, indicating that these layers were deposited after secession of fault movement.

Superimposed on the large (800 m) embayments are smaller 200 m long by 30 m wide scarps that appear to be controlled by the secondary, variable striking normal faults. These scarps expose the caprock and basement rock units and are present along the entire southern summit of the Atlantis Massif. Rubble from mass wasting events litters the slope below these arcuate scarps, indicating an extensive history of mass wasting (Figures 6 and 9a).

4.2. Detachment Shear Zone

Pervasive manganese coating on all exposed serpentinized peridotite and extant gabbroic lenses make these units difficult to distinguish from submersible observations. Therefore, these units are grouped

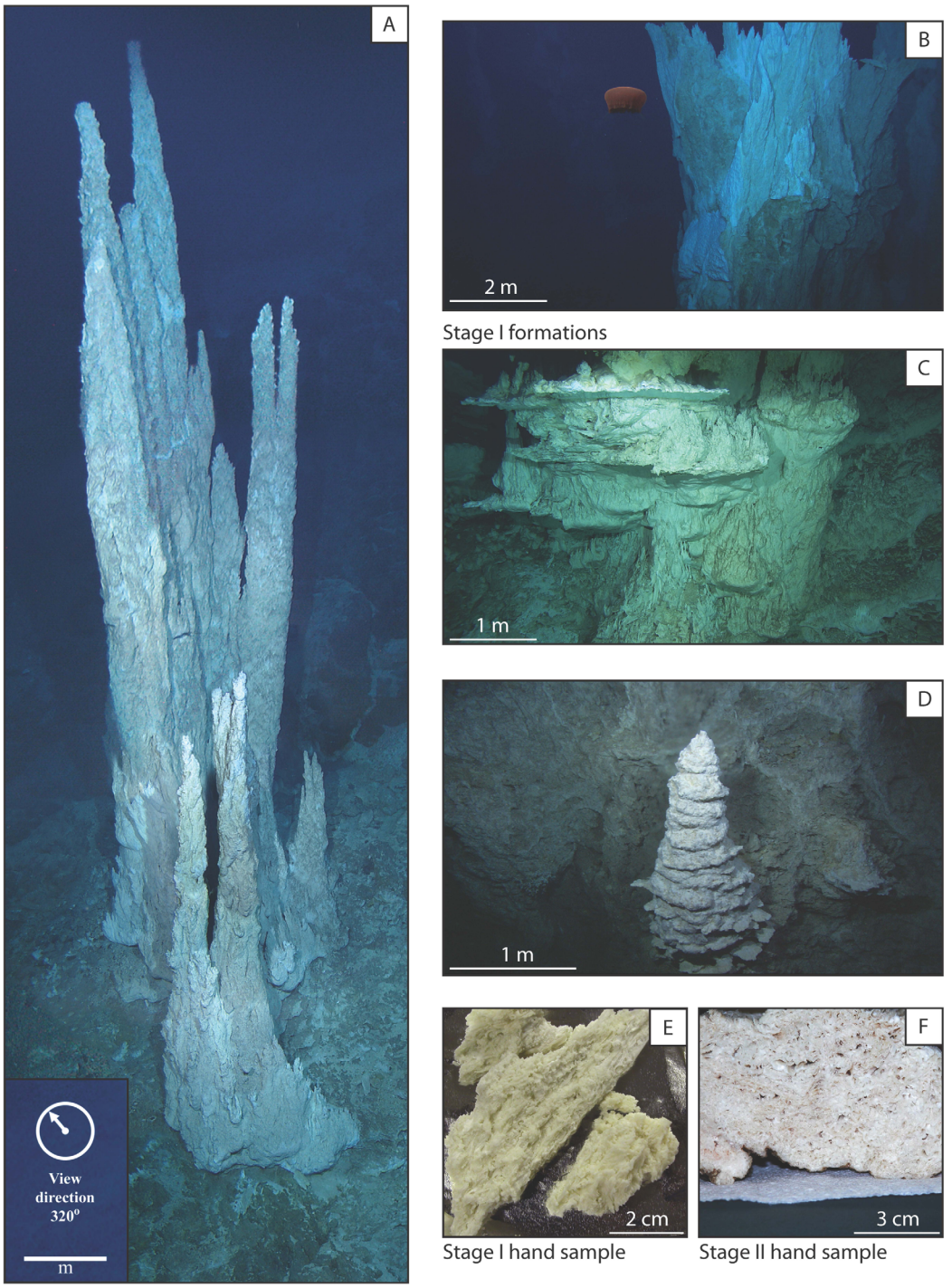

Figure 8. Examples of active and extinct hydrothermal carbonate at the LCHF. Clockwise from left: (a) the "Ryan" tower, due east of the main Poseidon complex, grows out of the base of a north-south trending fault scarp. Note the extensive carbonate talus surrounding this chimney complex. Photomosaic of this 14 m tall edifice is composed of images taken with the *ROV Hercules*. (b) The summit of the "Nature" tower 15 m east of Ryan. This structure hosts numerous active venting sites from both flanges and beehive-type structures at the summit. (c) Base of the IMAX tower on the northern flank of the Poseidon complex. It hosts myriad flanges with inverted pools of 60–70°C hydrothermal fluid. The mature structure extends ~10 m up the flank of Poseidon. (d) Beehive structure on the southern flank of Poseidon actively venting 91°C fluid, the highest temperature recorded at the LCHF. (e and f) Hand samples of Stage I and Stage II deposits, both recovered from the summit of Poseidon. Figures 8b–8d were taken with the *ROV Hercules*. All outcrop image locations are shown in Figure 9b.

together for mapping purposes in this study. This combined unit has a massive blocky structure, with fractures spaced 10 cm to 1 m apart (Figures 5d and 5f). With increased proximity to the high-strain zones, fractured block sizes are reduced and fractures are progressively oriented E-W with the DSZ fabric.

The seafloor expression of high-strain deformation along the detachment fault at the summit of the Atlantis Massif is uneven. The detachment zone is cut by numerous, high-angle normal faults that displace the deformation fabric and underlying massive serpentinite. The throw on these faults is difficult to determine because of a lack of definitive penetrating features within the complex high-strain fabric. However, given an overall mylonite thickness of 50–100 m, it is likely that these faults offset the deformation zone by $<$10 m.

4.3. Rubble Fields

Regions with steep slopes ($>$60°), especially proximal to two major high-angle normal faults and the main detachment fault, are dominated by massive serpentinite. Regions of less steep slopes (30–60°) bounding the LCHF are covered with pelagic carbonate and polymict rubble (Figure 10a). In the few regions of slopes with $<$30°, pelagic carbonate is much more abundant and cements the rubble that is sourced from all units upslope (Figure 10b). Some rubble regions are well lithified with varying degrees of hydrothermal and pelagic carbonate acting as the lithification agent. The degree of lithification depends on the distance from the LCHF venting region: lithification is highest adjacent to the LCHF.

Breccia deposits fall into two broad categories: (1) on the summit of the massif accumulations of exposed brecciated basalt, which were likely sourced from hanging wall blocks on the detachment surface [*Karson et al*., 2006] (Figure 9, orange unit; Figure 6d). (2) Immediately below the summit, most of the southern massif is covered in variably cemented breccia and unconsolidated talus produced by collapse of the OCC summit rocks and from the carbonate chimneys (Figure 9, yellow unit; Figure 10).

4.4. Hydrothermal Structures

The LCHF is a unique discovery, no other active field dominated by massive carbonate edifices has been found far off axis on an OCC. Other fields such as the TAG (Trans-Atlantic Geotraverse) [*Canales et al*., 2007], Rainbow [*Marques et al*., 2009], and Logatchev [*Petersen et al*., 2009] hydrothermal fields all host high-temperature sulfide deposits on mafic or ultramafic substrate that occur on or near the axial valley or axial bounding fault. In contrast to the Lost City carbonate towers that emit low to moderate temperature, high pH, low metal, and carbon-dioxide (CO_2)-absent fluids, the sulfide chimney fluids are acidic, metal rich, and contain high concentrations of CO_2 [*Charlou et al*., 2002; *Schmidt et al*., 2007]. Localized areas of fossiliferous carbonate sediments have been identified near the Rainbow hydrothermal field [*Lartaud et al*., 2011; *Andreani et al*., 2014]; however, to date, Lost City is the only known extensive, active carbonate hydrothermal field on an OCC.

The LCHF is perched along the southern wall of the Atlantis Massif at the intersection of a north-south trending, high-angle normal fault, and the main capping detachment fault (Figure 9a). The main part of the field is at a water depth of ~740 m. The field is directly atop a down-dropped block of pelagic carbonate caprock. The curved slab, composed of breccia overlying mylonitic serpentinite, is 250 × 400 m across and it is down dropped from the summit proper by ~70 m (Figure 9b). The core of the field is dominated by the Poseidon complex comprised of four adjoining massive edifices [*Kelley et al*., 2005]. Discrete chimneys, and chimney arrays extend from the Poseidon complex northward along a razorback ridge to just below the summit (water depth 745 m) (Figure 9b), and to the east, where hydrothermal fluids seep from a near-vertical, faulted cliff.

4.5. Central Lost City Field

The Poseidon edifice is a massive complex structure that is composed of four main edifices [*Kelley et al*., 2005]. The main tower rises 60 m above the seafloor and tapers to a summit 15 m in diameter. The summit is ~15 m taller than any surrounding structure [*Kelley et al*., 2001, 2005]. The bulk of the main tower is composed of indurated carbonate (Stage III) [*Ludwig et al*., 2006] heavily crosscut with more recent Stage II carbonate veins, indicating a long history of channel avulsion. The summit of the tower hosts two carbonate structures venting fluids at up to 88°C [*Ludwig et al*., 2006]. The flanks of Poseidon host several actively venting fissures, for example, a ~1 m tall "Beehive" structure venting fluids at up to 91°C (Figure 8d) and parasitic flanges with large stalagmite-type growths extending above them. One of these flanges, on the northern face of the Poseidon is called IMAX. It forms an impressive 30 m tall, multipronged chimney, which

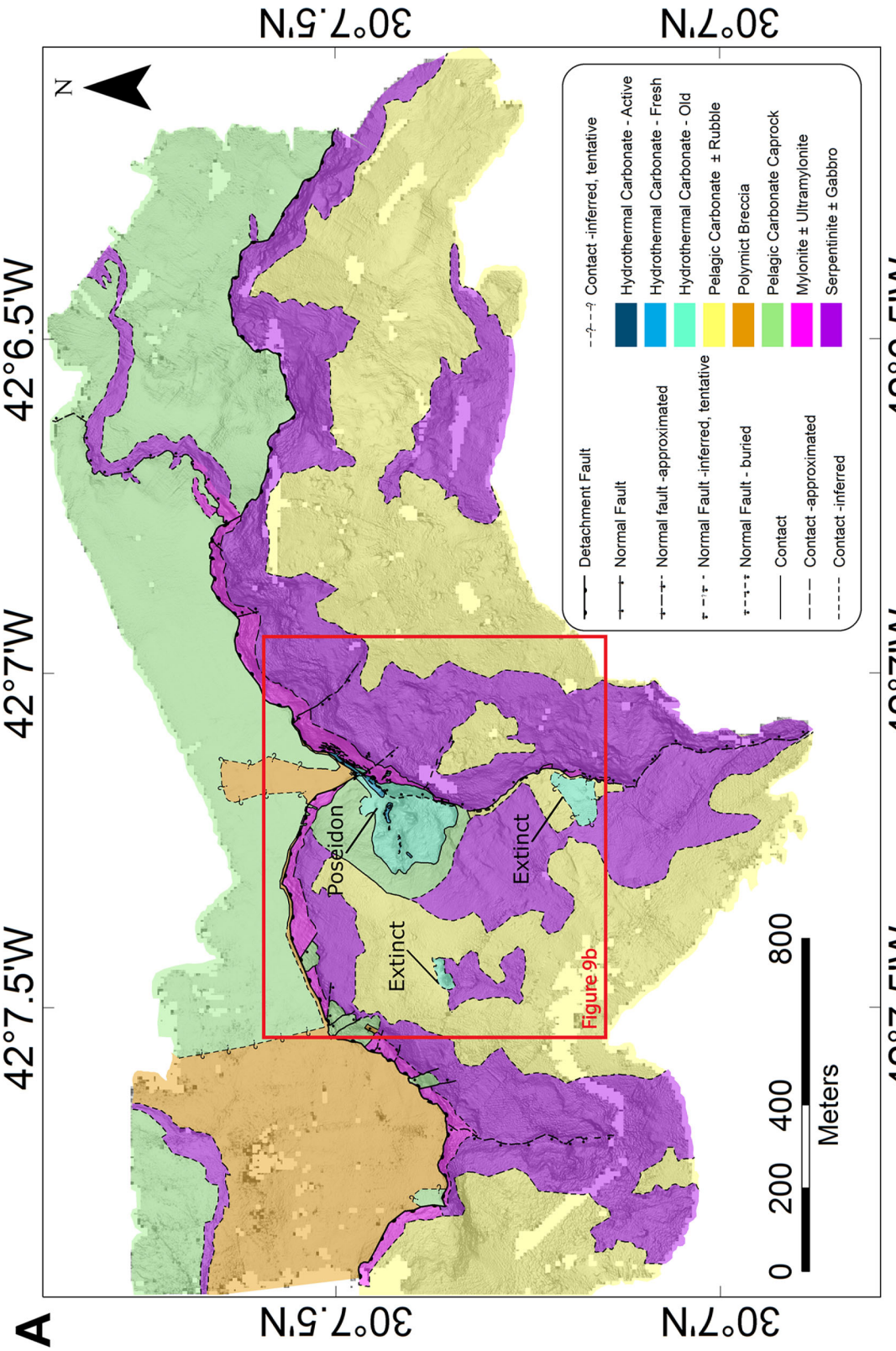

Figure 9. (continued)

is parasitically growing from the main trunk of Poseidon (Figure 8c) [*Kelley et al*., 2005]. In total, the Poseidon complex forms a linear E-W trending feature approximately 100 m in length.

Surrounding the Poseidon tower, the complex spreads out to the west as a series of hydrothermal structures that diminish rapidly in activity and size. The nearest deposits are separated from the Poseidon tower by a saddle filled with debris nearly entirely composed of large urchin spines (Chaff Basin). The western towers rise ~40 m above the seafloor and are composed of mature carbonate structures heavily crosscut with more recent carbonate veins that lack clear evidence of active venting (similar to Figure 7c).

Age dating, by *Ludwig et al*. [2011], of 67 carbonate deposits within the central LCHF yields modern to 120,000 years ages. Spatial-age relationships show that there is a strong tendency for the oldest samples to occur on the south side and down slope from the main Poseidon complex [*Ludwig et al*., 2011] (see Figure 10). Samples older than 4000 years were not documented to the north of the field (excluding the carbonate caprock). It should be noted, however, that distribution of dated samples was highly dependent on the ability to sample the deposits; the most well lithified, "older-looking" deposits, which typically also occurred in the southern portion of the field were difficult, if not impossible, to sample. Consequently for this study, the age dates and morphological interpretations were combined to examine the probable age distribution of various hydrothermal features.

4.5.1. Poseidon West

Continuing to the southwest and separated from the larger towers by ~30 m, there is a ridgeline of mature carbonate structures that extend all the way to the edge of the defined Poseidon carbonate deposit (Figure 9b). These towers are ≤20–30 m tall and are adjoined, forming a 75 m long ridge that progressively diminishes in size to the west. This ridge is heavily indurated, with substantial rounding, and overgrowth by benthic organisms.

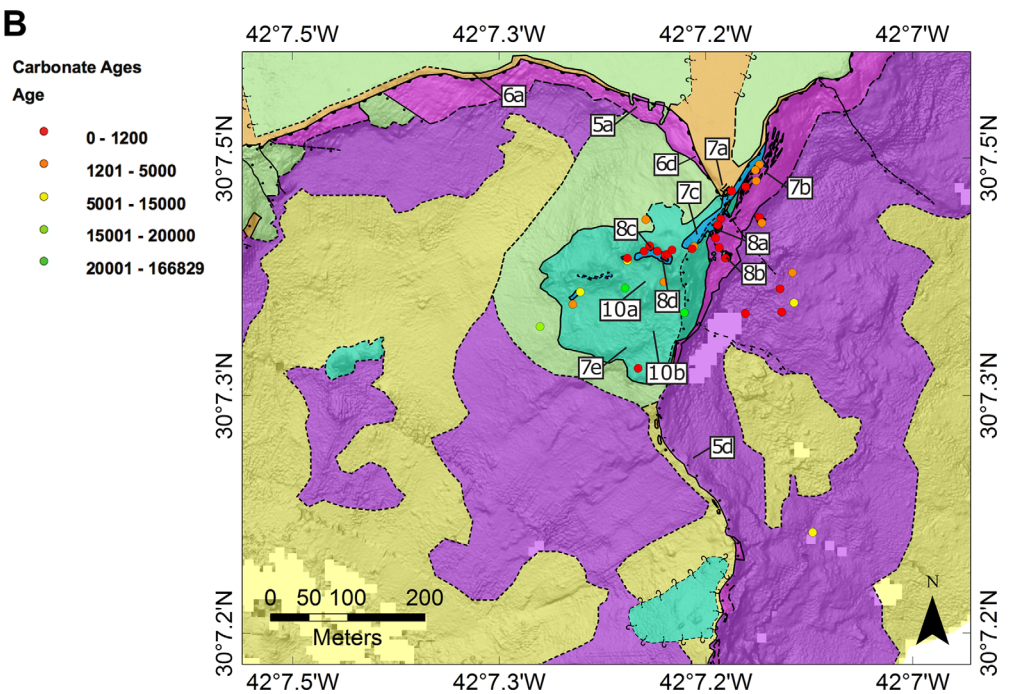

Figure 9. (a) Geologic map of the LCHF and adjacent Atlantis Massif (AM). (b) Detail of the LCHF proper, including the current LCHF and newly discovered fields. Carbonate age dates from *Ludwig et al*. [2006] are also shown as are locations of photographs in Figures 5–8. The geologic units are defined as follows: hydrothermal Carbonate—"Active"—actively venting, white, friable hydrothermal carbonate; "Fresh"—recently active carbonate, white and moderately friable, but with no visible venting. "Old"—grey, indurated and rounded carbonate with incorporated coral polyps; "Pelagic Carbonate ± Rubble"—pelagic carbonate with small clasts of serpentinite rubble, also as thin pelagic carbonate covering rubble, that are not part of the sediment cap; "Polymict Breccia"—carbonate-cemented polymict breccia with clasts of basalt, gabbro, and serpentine; "Pelagic Carbonate Caprock"—1 to 5 m thick, discontinuous pelagic carbonate on the summit of the AM, subhorizontal and infilling the polymict breccia surface; "Mylonite ± Ultramylonite"—50 to 100 m thick mylonitic serpentinite layer with low-angle, southwest-dipping anastomosing normal faults that define the detachment fault zone along the AM summit [*Karson et al*., 2006]. This layer contains lenses of highly deformed talc-tremolite schists that like represent metasomatically altered serpentinites [*Boschi et al*., 2006]; "Serpentinite ± Gabbro"—massive, blocky serpentinite with rare, irregular gabbroic lenses.

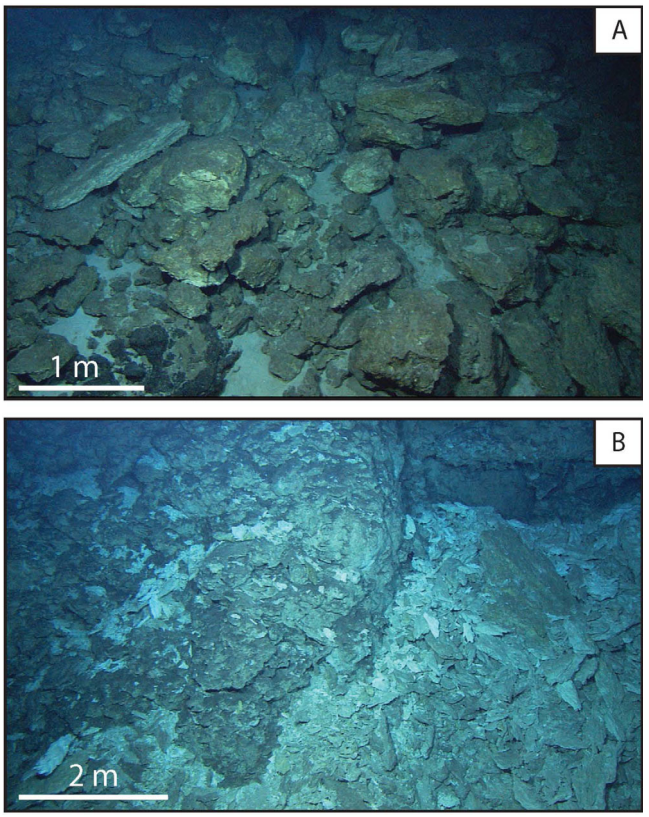

Figure 10. Outcrop images of hydrothermal carbonate rubble that litters the slope below the Lost City Hydrothermal Field. Images were taken with a down-looking camera on *Alvin* provided by D. Fornari, Woods Hole Oceanographic Institution.

4.5.2. Poseidon South

South of the Poseidon tower, there is a 60 m across expanse of carbonate pavement sporadically sedimented and covered in urchin spines. Here three extinct, mature carbonate towers form a deposit ~12 m in diameter. These towers are morphologically similar to the western-most deposits, but are disconnected from any other deposit. One hundred meters to the south, a row of short, 2–4 m tall, extinct structures mark the edge of the hydrothermal field. These towers form a chain spaced ~4 m apart and extend east-west for at least 70 m. The edifices are all heavily indurated and thickly overgrown with benthic fauna, with no evidence of recent venting activity (Figure 7e).

4.5.3. Poseidon East

East of the main Poseidon tower, a series of three carbonate towers extend to the edge of the high-angle normal fault scarp. These structures are actively venting, but at a much lower flow rate than those at the summit and on the sides of the Poseidon tower. Most of the activity in this region is marked by small flanges and miniature Stage I towers growing from the flank of a larger structure. Stages I–II hydrothermal deposits drape over the high-angle normal fault face, with numerous >1 m tall chimneys growing up through a thick deposit of hydrothermal talus The draping hydrothermal carbonate deposit extends to the base of the fault scarp, with only minor exposure of mylonite and serpentinite visible (Figure 10).

4.5.4. Poseidon North

Extending north along the fault scarp, a large array of 3–8 m tall towers form a continuous chain to within ~10 m of the Atlantis Massif summit. These structures are 1–2 m in diameter, Stages II–III carbonates with little visible venting. They host small deposits of snow-white carbonate.

All of the large hydrothermal carbonate structures within the field follow a rough E-W orientation, indicating that there may be an underlying high-angle, E-W trending normal fault that is controlling subsurface flow directly beneath the field. The region is covered in either hydrothermal carbonate or pelagic sediment, masking any fault expression.

4.6. Nascent Venting

The breccia and pelagic carbonate caprock are locally cut by fissures that are commonly in-filled with friable Stage I hydrothermal carbonate [*Kelley et al*., 2005; *Ludwig et al*., 2006]. The fissures are most pronounced on the edge of the massif summit (Figure 7a) adjacent to expansive blocks of down-dropped material from the summit. Although shimmering water was not commonly detected issuing from the fissures, it is likely that the hydrothermal deposits are young because (1) the fissures cut the caprock; (2) they are highly friable and snow white in color; (3) they are highly porous. The deposits occur only in fissures oriented east-west and north-south, where they form clusters that extend 1–5 m along strike, reaching ~15 cm in height. The variably in-filled fissures are localized at the summit of the massif and within ~100 m of steep escarpment marking the south face (Figure 9b).

Stage I deposits are also found northeast of the main field, directly emanating from mylonitic serpentinite (Figure 7b). These deposits typically occur in "sconce"-like deposits sympathetically oriented with the

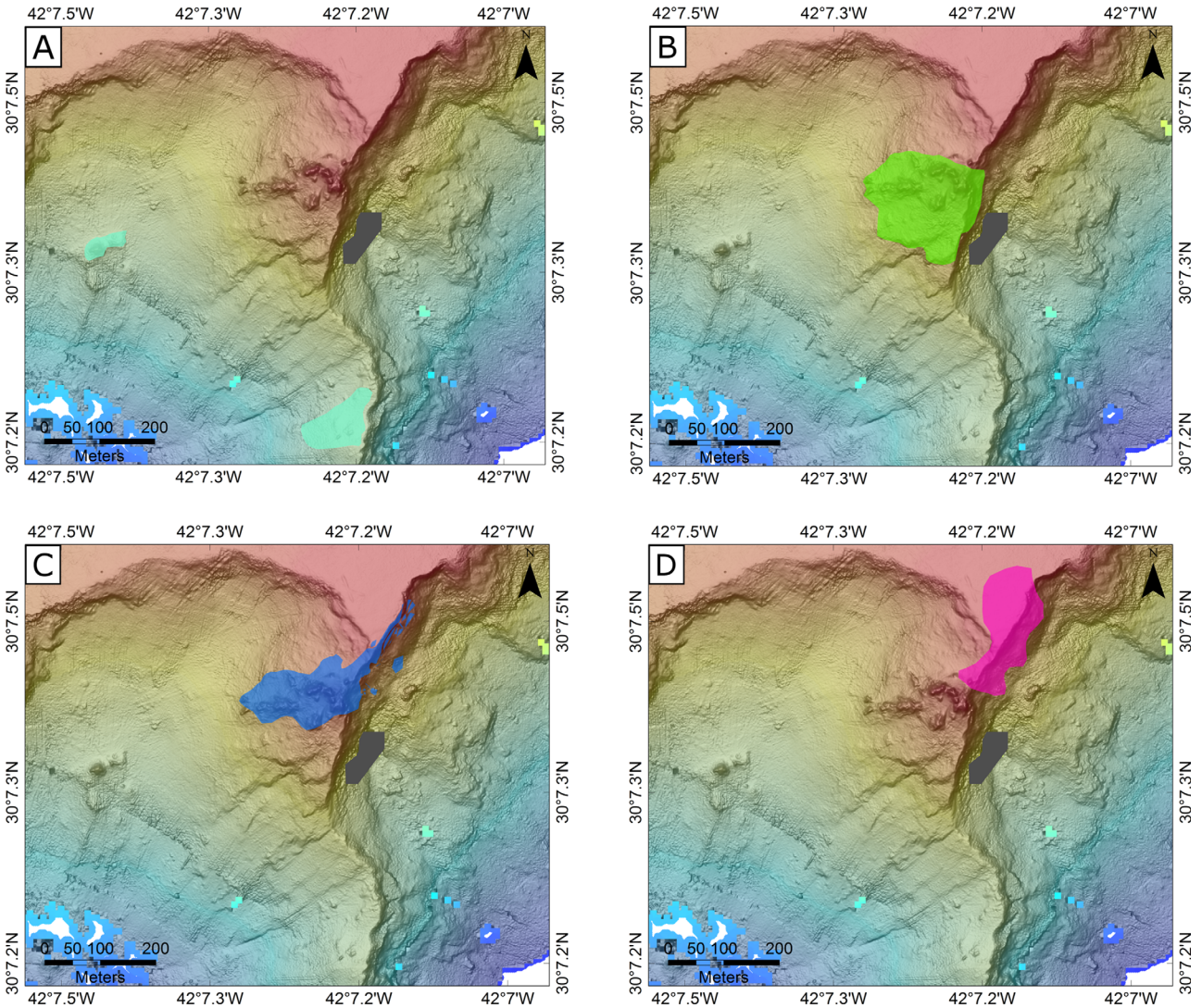

Figure 11. Field progression from a proposed future field location to the present location. The ancient (dark green) hydrothermal system is inferred from DSL-120 sidescan and geomorphologic interpretation. The old (light green) field location is based on observations of indurated carbonate mounds that represent an earlier generation of hydrothermal flow within the debris field of the current LCHF proper. The present (blue) field extent was mapped based on 2003 chimney locations. Future (pink) field progression is based on the current presence of nascent venting structures and the instability of the southern massif face. The black region to the East of the current field is a data gap.

pervasive regional mylonitic fabric. They are patchy in occurrence, and many are reminiscent of "upturned hands." In areas of long-term seepage, they form deposits > 1–4 m long.

4.7. Talus Field

An extensive skirt of extinct carbonate debris defines the flanks of the Poseidon complex. Most of the debris pieces are >1 m across and are extinct, variably lithified portions of carbonate chimneys. On the north side of Poseidon, massive carbonate slabs several meters across and variably covered with smaller fragments form an extensive talus field. On the south side of the edifice, thick talus deposits of extinct chimneys litter the slopes immediately beneath the field (Figure 10). The central hydrothermal structures are relatively unstable and prone to collapse, allowing for the buildup of a significant apron of debris around active or recently extinct structures. The rare, massive discrete slabs likely reflect past catastrophic chimney collapse.

4.8. Extinct Fields

Two relict fields were discovered during detailed investigation of dive imagery, side scan data, and bathymetry (Figure 9b). The first field is downslope 300 m and to the west of the LCHF. It covers an area ~120 m × 80 m, at a depth range of 1000–1065 m. The second extinct field is 450 m west-southwest of Poseidon at a

Table 1. Selected Volatiles and Hydrocarbons in Ultramafic/Gabbroic Hydrothermal Systems

Site	T°C	H_2 (mmol/kg)	CH_4 (mmol/kg)	CO_2 (mmol/kg)	C_2H_6 ethane (nmol/kg)	C_2H_4 ethylene (nmol/kg)	C_3H_8 propane (nmol/kg)	$\delta^{13}CH_4$ ‰
Rainbow	323–370[a–c]	4.8–16[a,c]	2.50[c]	10.1–30[a–c]	1097[c]	n.m	48[c]	−15.8 to 17.7[b,c]
Logatchev[c]	352	12	2.10	2.5	n.m	n.m	n.m	−13.6
Lost City[d]	44–90	0.48–14.38	1.03–1.98	0.0001–0.026	910–1790	2–21	73–160	−9.4 to 13.6
Endeavour	300–380	0.12–1.38[d]	3.40[e]	6.14–110.65[f]	n.m	n.m	n.m	−51.7[e]
EPR[g]	307–396	0.21–27.07	−0.05 to 0.16	44.76–220.0	n.m	n.m	n.m	19.9–34.6

[a]*Seyfried et al.* [2011].
[b]*Konn et al.* [2009].
[c]*Charlou et al.* [2002] ($\delta^{13}CO_2 = -3.15‰$ Rainbow; −4.3 Logatchev).
[d]*Proskurowski et al.* [2006]
[e]*Lilley et al.* [2003].
[f]*Proskurowski et al.* [2004] ($\delta^{13}CO_2 = -6.8$ to 9.85‰).
[g]*Proskurowski et al.* [2008] ($\delta^{13}CO_2 = -3.7$ to 4.36‰); n.m. indicates not measured; EPR = East Pacific Rise.

water depth of ~1000 m. This extinct deposit is identified by a 15 m tall, roughly conical feature, and several towers 35 m to the east of the main tower. The morphology and appearance in side scan are remarkably similar to Poseidon. A single CTD cast over the latter field showed no evidence of active flow, though direct imaging is required to confirm that the field is extinct. None of the dive programs in this study covered either location. However, a Russian expedition aboard the R/V *Academik Keldysh* is reported to have discovered an ancient relict field (Lost Village) to the south of the main LCHF [*Dara et al*., 2009]. That study, however, does not provide navigation information to confirm or reject this identification.

5. Discussion

Results of detailed bathymetric, direct imaging, and side scan analyses provide the foundation for a new model of the geologic and hydrothermal evolution of the LCHF and upper Atlantis Massif summit. The evolution of the vent field is constrained by structural and unit relationships revealed by the high-resolution geologic map, age dates of carbonate deposits from *Ludwig et al*. [2011], and the inferred tectonic structure of the Atlantis Massif. The evolutionary model proposed for the Lost City system is one in which controlling faults progressively migrate to the north with exhumation of the Atlantis Massif and continued development of embayments that expose fresh wall rock. This model is predicated on the assumption that the extinct fields located in this study were not venting at the same time as the current LCHF. Additional age dating is required to test this model.

The extinct fields discovered in this study lie 300 m south and 450 m southwest of the LCHF and are separated from the currently active field by extensive talus slopes. The two fields are at a depth of 1000 and 1050 m, respectively, and extend as far as 750 m downslope from the current locus of hydrothermal outflow. These results are interpreted to indicate that venting and field development have migrated to the north intermittently due to punctuated changes in flow channels associated with faulting and mass wasting events (Figure 11). Based on CTD results of the most western field in which a water column anomaly was absent, it is thought that this deposit is inactive.

The deeper ancient field likely occupied a similar position to the current LCHF at the intersection of a detachment fault and a near-vertical normal fault. The morphology of the relict field (Figure 11a) indicates that it is possibly on a down-dropped block of carbonate caprock. It is proposed that due to punctuated mass wasting events, the plumbing system to the field was disrupted, resulting in the shutdown of the old field. Other mechanisms for the termination of hydrothermal flow (i.e., cementation of the fluid flow pathway or depletion of the hydrothermal heat source) are deemed less likely given the clear structural control on the current LCHF and the similar down-dropped placement of the southern field.

Following cessation of flow at the southern, now deeper field, venting shifted to the north at the present LCHF site (Figure 11b). Initial venting was focused at the (now) extinct chimneys on the southern edge of the present carbonate deposit, where the oldest carbonate dates were measured at ~169,000 to 120,000 years in age [*Ludwig et al*., 2011]. Over the next ~100,000 years, venting progressively moved to the north where the Poseidon edifice is now located and where the youngest carbonate dates are obtained (4800–17 years in age) (Figures 11b and 11c).

Venting at the current LCHF is strongly controlled by the N-S striking normal faults as demonstrated by the locus of venting perched directly on the faults. These faults are interpreted to predate the exhumation of the detachment fault because they do not offset the detachment fault surface. The final generation of faulting/fracturing is the NW-SE trending faults that crosscut both the detachment surface and the older N-S trending faults. There is very little relative offset on these features, which may indicate that they are related to incipient fracturing and expansion of the detachment surface.

Nascent venting systems are developing in the far northeast of the field along the steep eastern wall, and on the down-dropped block to the east. Shallower and more northerly crosscutting arrays of carbonate-filled fissures that cut the caprock (Figure 7a) reflect either expansion of LCHF venting, or initiation of a new field on the summit of the massif. This interpretation is supported by the results of *Ludwig et al*. [2011], which show that three carbonate deposits formed within the caprock range in age from 52 ± 13 to 1061 ± 844 years. The close proximity of the angular fissure sets to the edge of the near-vertical cliff bounding the summit and to large, calved off angular, down-dropped blocks of breccia and carbonate caprock immediately below the summit, are consistent with formation by expansion fractures. Hence, it is possible that they represent nascent venting features on the summit of the massif and the beginning of a new plumbing system for the next Lost City field (Figure 11d).

In contrast to other known hydrothermal systems associated with OCCs, the LCHF is the furthest off axis, has the highest pH values measured in a mid-ocean ridge submarine venting environment, and has fluid chemistry that is a hallmark of serpentinization reactions at depth; e.g., very low metals, low CO_2, and high elevated CH_4 and H_2 concentrations (Table 1) [*Kelley et al*., 2005; *Proskurowski et al*., 2008]. Although the TAG field is similar in age to Lost City [*Lalou et al*., 1995], it is a high-temperature black and white smoker system hosted in basalt on the hanging wall block with fluid sourced along the active detachment fault [*Canales et al*., 2007; *deMartin et al*., 2007]. Fluid signatures are consistent with a basaltic-gabbroic dominated system with low pH values, moderate CO_2 concentrations, and low CH_4 and H_2 concentrations. Both Logatchev and Rainbow are high-temperature black smoker systems hosted on variable mixtures of ultramafic, gabbroic, and basaltic material. Logatchev is situated $\sim$7 km from the spreading axis on the inner rift valley wall [*Petersen et al*., 2009]. It is one of the best studied systems on the MAR where active high-temperature serpentinization reactions occur at depth [*Pedersen et al*., 2010]. Here it is thought that low-angle detachment faults serve as fluid flow channels with gabbroic intrusions as the heat sources to drive flow. The Rainbow hydrothermal field is hosted on a fault-bounded block of ultramafic rocks with lesser basaltic material and hosts 11 major vent sites [*Charlou et al*., 2002, 2010; *Marques et al*., 2007]. Fluid chemistries at both Logatchev and Rainbow reflect the influence of high-temperature subsurface reactions involving both gabbroic and ultramafic rocks. These characteristics include high-temperature venting of high pH, metal-rich, high CO_2 fluids with values similar to those of basaltic-dominated systems such as Endeavour and the East Pacific Rise. However, they also include high CH_4 and H_2 concentrations reflecting an ultramafic influence (Table 1) [*Charlou et al*., 2002; *Schmidt et al*., 2007; *Konn et al*., 2009; *Seyfried et al*., 2011]. From these data, it is clear that LCHF is an end-member for hydrothermally active systems associated with mid-ocean ridge environments.

6. Conclusion

The LCHF is a long-lived hydrothermal system ($>$120,000 years) [*Ludwig et al*., 2011] that has gone through numerous discrete stages of development. Given the discovery of multiple, currently unexplored fields that are inactive and spatially separated from the present locus of venting, and because prior age dating focused on samples most easily recovered, it is suggested that hydrothermal venting on the Atlantis Massif is much longer lived than the current age dating indicates. The newly identified extinct fields are of unknown age, but are hypothesized to be older than the current venting field, and possibly hold information on the initiation of hydrothermal flow on the Atlantis Massif. Direct sampling of these extinct features is essential to forward our understanding of the development and evolution of both hydrothermal flow and associated microbial assemblages in this area [*Brazelton et al*., 2010].

The ubiquity of massifs [*Blackman et al*., 2009] and exposures of variably altered and deformed peridotites along slow and ultraslow spreading ridges allows the assumption that additional Lost City-type fields are present within these environments. The discovery of the LCHF on the Atlantis Massif was a fortuitous

occurrence. A focused exploration of candidate massif structures is required to expand our understanding of these features from a single example to a global phenomenon with currently unconstrained impacts on marine biogeochemical cycles.

Acknowledgments
We gratefully acknowledge the reviewers and Editors for their insightful comments on this paper. This work was supported by an NSF grant (OCE 0137206) and by a 2005 NOAA-Ocean Exploration Award to Kelley. G.F.G. acknowledges support from ETH grant 0-20890-01 and Swiss SNF grants 2100-068055 and 200020-107620. Data for this publication are available at www.lostcity.washington.edu/resources and at Marine Geoscience Data System (http://www.marine-geo.org/index.php).

References

Andreani, M. A., A. Escartin, A. Delacour, B. Illdefonse, M. Godard, J. Dyment, A. E. Fallick, and Y. Fouquet (2014), Tectonic structure, lithology, and hydrothermal signature of the Rainbow massif (Mid-Atlantic Ridge 36°14′N), *Geochem. Geophys. Geosyst.*, *15*, 3543–3571, doi:10.1002/2014GC005269.

Blackman, D., D. Kelley, and J. Karson (2015), *Processed Gridded DSL-120 Sidescan Sonar Data From the Mid-Atlantic Ridge Spreading Center Acquired During the Atlantis Expedition AT03-60 (2000)*, Integrated Earth Data Appl., in Palisades, N. Y. doi:10.1594/IEDA/321918.

Blackman, D. K., et al. (2002), Geology of the Atlantis Massif (Mid-Atlantic Ridge, 30°N): Implications for the evolution of an ultramafic oceanic core complex, *Mar. Geophys. Res.*, *23*, 443–469, doi:10.1023/B:MARI.0000018232.14085.75.

Blackman, D. K., G. D. Karner, and R. C. Searle (2008), Three-dimensional structure of oceanic core complexes: Effects on gravity signature and ridge flank morphology, Mid-Atlantic Ridge, 30°N, *Geochem. Geophys. Geosyst.*, *9*, Q06007, doi:10.1029/2008GC001951.

Blackman, D. K., J. P. Canales, and A. Harding(2009), Geophysical signatures of oceanic core complexes, *Geophys. J. Int.*, *178*, 593–613, doi:10.1111/j.1365-246X.2009.04184.x.

Blackman, D. K., et al. (2011), Drilling constraints on lithospheric accretion and evolution at Atlantis Massif, Mid-Atlantic Ridge 30N, *J. Geophys. Res.*, *116*, B07103, doi:10.1029/2010JB007931.

Boschi, C., G. L. Früh-Green, A. Delacour, J. A. Karson, and D. S. Kelley (2006), Mass transfer and fluid flow during detachment faulting and development of an oceanic core complex, Atlantis Massif (MAR 30°N), *Geochem. Geophys. Geosyst.*, *7*, Q01004, doi:10.1029/2005GC001074.

Brazelton, W. J., M. O. Schrenk, D. S. Kelley, and J. A. Baross (2006), Methane- and sulfur-metabolizing microbial communities dominate the lost city hydrothermal field ecosystem, *Appl. Environ. Microbiol.*, *72*(9), 6257–6270, doi:10.1128/AEM.00574-06.

Brazelton, W. J., K. Ludwig, M. L. Sogin, E. N. Andreishcheva, D. S. Kelley, C.–C. Shen, R. L. Edwards, and J. A. Baross (2010), Archaea and bacteria with surprising microdiversity show shifts in dominance over 1,000-year time scales in hydrothermal chimneys, *Proc. Natl. Acad. Sci. U. S. A.*, *107*(4), 1612–1617, doi:10.1073/pnas.0905369107.

Buck, W. R., L. L. Lavier, and A. N. B. Poliakov (2005), Modes of faulting at mid-ocean ridges, *Nature*, *434*, 719–723, doi:10.1038/nature03358.

Buck, W. R. (1988), Flexural rotation of normal faults, *Tectonics*, *7*, 959–973, doi:10.1029/TC007i005p00959.

Canales, J. P., R. A. Sohn, and B. J. deMartin (2007), Crustal structure of the Trans-Atlantic Geotraverse (TAG) segment (Mid-Atlantic Ridge, 2610′N): Implications for the nature of hydrothermal circulation and detachment faulting at slow spreading ridges, *Geochem. Geophys. Geosyst.*, *8*, Q08004, doi:10.1029/2007GC001629.

Cann, J. R., D. K. Blackman, D. K. Smith, E. McAllister, B. Janssen, S. Mello, E. Avgerinos, A. R. Pascoe, and J. Escartin (1997), Corrugated slip surfaces formed at ridge–transform intersections on the Mid-Atlantic Ridge, *Nature*, *385*, 329–332, doi:10.1038/385329a0.

Cannat, M., Y. Lagabrielle, H. Bougault, J. Casey, N. de Coutures, L. Dmitriev, and Y. Fouquet (1997), Ultramafic and gabbroic exposures at the Mid-Atlantic Ridge: Geological mapping in the 15°N region, *Tectonophysics*, *279*, 193–213, doi:10.1016/S0040-1951(97)00113-3.

Caress, D. W., and D. N. Chayes (2014), *MB-System: Mapping the Seafloor*, Scripps Oceanographic, Moss Landing, Calif. [Available at http://www.mbari.org/data/mbsystem and http://www.ldeo.columbia.edu/res/pi/MB-System.]

Charlou, J. L., J. P. Donval, Y. Fouquet, P. Jean-Baptiste, and N. Holm (2002), Geochemistry of high H_2 and CH_4 vent fluids issuing from ultramafic rocks at the Rainbow hydrothermal field (36°14′N,MAR), *Chem. Geol.*, *191*, 345–359, doi:10.1016/S0009-2541(02)00134-1.

Charlou, J. L., J. P. Donval, C. Konn, H. Ondreas, and Y. Fouquet (2010), High production and fluxes of H_2 and CH_4 and evidence of abiotic hydrocarbon synthesis by serpentinization in ultramafic-hosted hydrothermal systems on the Mid-Atlantic Ridge, in *Diversity of Hydrothermal Systems on Slow Spreading Ocean Ridges*, vol. 188, edited by P. Rona, C. Devey, and B. Murton, pp. 265–296, AGU, Washington, D. C.

Dara, O. M., T. G. Kuz'mina, and A. Y. Lein (2009), Mineral associations of the Lost Village and Lost City hydrothermal fields in the North Atlantic, *Oceanology*, *49*(5), 688–696, doi:10.1134/S0001437009050105.

Delacour, A., G. L. Früh-Green, M. Frank, M. Gutjahr, and D. S. Kelley (2008), Sr- and Nd-isotope geochemistry of the Atlantis Massif (30°N, MAR): Implications for fluid fluxes and lithospheric heterogeneity, *Chem. Geol.*, *254*, 19–35, doi:10.1016/j.chemgeo.2008.05.018.

deMartin, B. J., R. A. Sohn, J. P. Canales, and S. E. Humphris (2007), Kinematics and geometry of active detachment faulting beneath the Trans-Atlantic Geotraverse (TAG) hydrothermal field on the Mid-Atlantic Ridge, *Geology*, *35*(8), 711–714.

Dick, H. J. B. (1989), Abyssal peridotites, very slow spreading ridges and ocean ridge magmatism, *Geol. Soc. Spec. Publ.*, *42*(1), 71–105, doi:10.1144/GSL.SP.1989.042.01.06.

Escartín, J., and M. Cannat (1999), Ultramafic exposures and the gravity signature of the lithosphere near the Fifteen-Twenty Fracture Zone (Mid-Atlantic ridge, 14°-16.5°N), *Earth Planet. Sci. Lett.*, *171*, 411–424. doi:10.1016/S0012-821X(99)00169-7.

Escartín, J., D. K. Smith, J. Cann, H. Schouten, C. H. Langmuir, and S. Escrig (2008), Central role of detachment faults in accretion of slow-spreading oceanic lithosphere, *Nature*, *455*, 790–794, doi:10.1038/nature07333.

Expedition Scientific Party (2005), Oceanic core complex formation, Atlantis Massif—oceanic core complex formation, Atlantis Massif, Mid-Atlantic Ridge: drilling into the footwall and hanging wall of a tectonic exposure of deep, young oceanic lithosphere to study deformation, alteration, and melt generation, Prelim. Rep. Integrated Ocean Drill. Program, 304.

Ferrini, V., D. J. Fornari, T. Shank, M. Tivey, D. S. Kelley, D. Glickson, S. M. Carbotte, J. Howland, L. L. Whitcomb, and D. Yoerger (2004), Very high resolution bathymetric mapping at the ridge 2000 integrated study sites: Acquisition and processing protocols developed during recent Alvin field programs to the east Pacific rise and Juan de Fuca Ridge, *Eos Trans. AGU*, *85*(47), Fall Meet. Suppl., Abstract B13A-0162.

Früh-Green, G. L., D. S. Kelley, S. M. Bernasconi, J. A. Karsen, K. A. Ludwig, D. A. Butterfield, C. Boschi, and G. Proskurowski (2003), 30,000 years of hydrothermal activity at the lost city vent field, *Science*, *301*, 495–498, N. Y.

Holm, N. G. (2012), The significance of Mg in prebiotic geochemistry, *Geobiology*, *10*, 269–279, doi:10.1111/j.1472-4669.2012.00323.x.

Holm, N. G., and J. L. Charlou (2001), Initial indications of abiotic formation of hydrocarbons in the Rainbow ultramafic hydrothermal system, Mid-Atlantic Ridge, *Earth Planet. Sci. Lett.*, *191*, 1–8, doi:10.1016/S0012-821X(01)00397-1.

Howard, K. A., B. E. John, and C. F. Miller (1987), Metamorphic core complexes, Mesozoic ductile thrusts, and Cenozoic detachments: Old Woman Mountains—Chemehuevi Mountains transect, California and Arizona, *Geol. Soc. Amer.*, Fieldtrip Guidebook, pp. 365–382, Ariz. Bur. of Geol. and Mines Technol.

Hsu, H.-W., et al. (2015), Ongoing hydrothermal activities within Enceladus, *Nature*, *519*(7542), 207–210, doi:10.1038/nature14262.

Illdefonse, B., et al. (2007), Oceanic core complexes and crustal accretion at slow-speading ridges, *Geology*, *35*, 623–626, doi:10.1130/G23531A.1.

John, B. E., and M. J. Cheadle (2010), Deformation and alteration associated with oceanic and continental detachment fault systems: Are they similar?, in *Diversity of Hydrothermal Systems on Slow Spreading Ocean Ridges*, vol. 188, pp. 175–205, AGU, Washington, D. C., doi: 10.1029/2008GM000772.

Karson, J. A. (1990), Seafloor spreading on the Mid-Atlantic Ridge: Implications for the structure of ophiolites and oceanic litho-sphere produced in slow-spreading environments, in *Ophiolites and Oceanic Crustal Analogues: Proceedings of the Symposium "Troodos 1987"*, edited by J. Malpas et al., pp. 125–130, Geol. Surv. Dep., Nicosia.

Karson, J. A., G. L. Früh-Green, D. S. Kelley, E. A. Williams, D. R. Yoerger, and M. Jakuba (2006), Detachment shear zone of the Atlantis Massif core complex, Mid-Atlantic Ridge, 30°N, *Geochem. Geophys. Geosyst.*, *7*, Q06016, doi:10.1029/2005GC001109.

Kelley, D. S., and T. M. Shank (2010), Hydrothermal systems: A decade of discovery in slow spreading environments, in *Diversity of Hydrothermal Systems on Slow Spreading Ocean Ridges*, vol. 188, pp. 369–407, AGU, Washington, D. C., doi:10.1029/2010GM000945.

Kelley, D. S., et al. (2001), An off-axis hydrothermal vent field near the Mid-Atlantic Ridge at 30 degrees N, *Nature*, *412*, 145–149, doi: 10.1038/35084000.

Kelley, D. S., et al. (2005), A serpentinite-hosted ecosystem: The Lost City hydrothermal field, *Science*, *307*(2005), 1428–1434, doi:10.1126/ science.1102556.

Kelley, D. S., J. Karson, and D. Yoerger (2015), *Bathymetry Grid From the Atlantis Massif Acquired in 2003 With the AUV ABE During the Lost City Expedition, Atlantis Cruise AT07-34*, Integrated Earth Data Appl., Palisades, N. Y., doi:10.1594/IEDA/321847.

Konn, C., J. L. Charlou, J. P. Donval, N. G. Holm, F. Dehairs, and S. Bouillon (2009), Hydrocarbons and oxidized organic compounds in hydro-thermal fluids from Rainbow and Lost City ultramafic-hosted vents, *Chem. Geol.*, *258*, 299–314.

Lalou, C., J.-L. Reyss, E. Brichet, P. A. Rona, and G. Thompson (1995), Hydrothermal activity on a 105 year scale at a slow- spreading ridge, TAG hydrothermal field, Mid-Atlantic Ridge 26?N, *J. Geophys. Res.*, *100*, 17,855–17,862.

Lang, S. Q., D. A. Butterfield, M. S. Schulte, D. S. Kelley, and M. D. Lilley (2010), Elevated concentrations of formate, acetate and dissolved organic carbon found at the lost city hydrothermal field, *Geochim. Cosmochim. Acta*, *74*, 941–952.

Lang, S. Q., G. L. Früh-Green, S. M. Bernasconi, M. D. Lilley, G. Proskurowski, S. Méhay, and D. A. Butterfield (2012), Microbial utilization of abiogenic carbon and hydrogen in a serpentinite-hosted system, *Geochim. Cosmochim. Acta*, *92*, 82–99.

Lartaud, F., C. T. S. Little, M. De Rafelis, G. Bayon, J. Dyment, B. Ildefonse, Y. Fouquet, F. Gaill, and N. Le Bris (2011), Fossil evidence for serpentinization fluids fueling chemosynthetic assemblages, *Proc. Natl. Acad. Sci. U. S. A.*, *108*, 7968–7703, doi:10.1073/pnas. 1009383108.

Lilley, M. D., D. A. Butterfield, J. E. Lupton, and E. J. Olson (2003), Magmatic events can produce rapid changes in hydrothermal vent chem-istry, *Nature*, *422*, 878–881.

Ludwig, K. A., D. S. Kelley, D. A. Butterfield, B. K. Nelson, and G. L. Früh-Green (2006), Formation and evolution of carbonate chimneys at the Lost City Hydrothermal Field, *Geochim. Cosmochim. Acta*, *70*, 3625–3645, doi:10.1016/j.gca.2006.04.016.

Ludwig, K. A., C. C. Shen, D. S. Kelley, H. Cheng, and R. L. Edwards (2011), U-Th systematics and 230Th ages of carbonate chimneys at the Lost City Hydrothermal Field, *Geochim. Cosmochim. Acta*, *75*(7), 1869–1888, doi:10.1016/j.gca.2011.01.008.

MacLeod, C. J., R. C. Searle, B. J. Murton, J. F. Casey, C. Mallows, S. C. Unsworth, K. L. Achenbach, and M. Harris (2009), Life cycle of oceanic core complexes, *Earth Planet. Sci. Lett.*, *287*(3-4), 333–344, doi:10.1016/j.epsl.2009.08.016.

MacLeod, C. J., J. Carlut, J. Escartín, H. Horen, and A. Morris (2011), Quantitative constraint on footwall rotations at the 1545N oceanic core complex, Mid-Atlantic Ridge: Implications for oceanic detachment fault processes, *Geochem. Geophys. Geosyst.*, *12*, Q0AG03, doi:10.1029/2011GC003503.

Martin, W., J. Baross, D. S. Kelley, and M. J. Russell (2008), Hydrothermal vents and the origin of life, *Nat. Rev. Microbiol.*, *6*(II), 805–814, doi:10.1038/nrmicro1991.

Marques, A. F. A., F. J. A. S. Barriga, and S. D. Scott (2007), Sulfide mineralization in an ultramafic-rock hosted seafloor hydrothermal system: From serpentinization to the formation of Cu-Zn-(Co)-rich massive sulfides, *Mar. Geol.*, *245*, 20–39, doi:10.1016/j.margeo.2007.05.007.

Marques, A. F. A., S. D. Scott, M. P. Gorton, F. J. A. S. Barriga, and Y. Fouquet (2009), Pre-eruption history of enriched MORB from the Menez Gwen (37 50′ N) and Lucky Strike (37|7′N) hydrothermal systems, Mid-Atlantic Ridge, *Lithos*, *112*, 18–39.

McCaig, A. M., R. A. Cliff, J. Escartin, A. E. Fallick, and C. J. MacLeod (2007), Oceanic detachment faults focus very large volumes of black smoker fluids, *Geology*, *35*, 935–938, doi:10.1130/G23657A.1.

McCollom, T. M., and W. Bach (2009), Thermodynamic constraints on hydrogen generation during serpentinization of ultramafic rocks, *Geochim. Cosmochim. Acta*, *73*(3), 856–875, doi:10.1016/j.gca.2008.10.032.

McCollom, T. M., and J. S. Seewald (2006), Carbon isotope composition of organic compounds produced by abiotic synthesis under hydro-thermal conditions, *Earth Planet. Sci. Lett.*, *243*, 74–84, doi:10.1016/j.epsl.2006.01.027.

McCollom, T. M., and J. S. Seewald (2013), Serpentinites, hydrogen, and life, *Elements*, *9*, 129–134, doi:10.2113/gselements.9.2.129.

Morris, A., J. S. Gee, N. Pressling, B. E. John, C. J. MacLeod, C. B. Grimes, and R. C. Searle (2009), Footwall rotation in an oceanic core complex quanti-fied using reoriented Integrated Ocean Drilling Program core samples, *Earth Planet. Sci. Lett.*, *287*(1-2), 217–228, doi:10.1016/j.epsl.2009.08.007.

Mutter, J. C., and J. A. Karson (1992), Structural processes at slow-spreading ridges, *Science*, *257*, 627–634.

O'Hanley, D. S. (1996), *Serpentinites—Records of Tectonic and Petrological History, Oxford Monogr. Geol. Geophys.*, vol. 34, 277 pp., Oxford Univ. Press, N. Y.

Olive, J.-A., M. D. Behn, and B. E. Tucholke (2010), The structure of oceanic core complexes controlled by the depth distribution of magma emplacement, *Nat. Geosci.*, *3*(7), 491–495, doi:10.1038/ngeo888.

Pedersen, R. B., I. H. Thorseth, T. E. Nygård, M. D. Lilley, and D. S. Kelley (2010), Hydrothermal activity at the arctic Mid-Ocean Ridges, in *Diversity of Hydrothermal Systems on Slow Spreading Ocean Ridges*, vol. 188, pp. 67–89, AGU, Washington, D. C., doi:10.1029/ 2008GM000783.

Petersen, S., K. Kuhn, T. Kuhn, N. Augustin, R. Hékinian, L. Franz, and C. Borowski (2009), The geological setting of the ultramafic-hosted Logatchev hydrothermal field (14drothe Mid-Atlantic Ridge) and its influence on massive sulfide formation, *Lithos*, *112*, 40–56, doi:10.1016/j.lithos.2009.02.008.

Proskurowski, G., M. D. Lilley, and T. A. Brown (2004), Isotopic evidence of magmatism and seawater bicarbonate removal at the endeavour hydrothermal system., *Earth Planet. Sci. Lett.*, *225*, 53–61.

Proskurowski, G., M. D. Lilley, D. S. Kelley, and E. J. Olson (2006), Low temperature volatile production at the Lost City Hydrothermal Field, evidence from a hydrogen stable isotope geothermometer, *Chem. Geol.*, *229*, 331–343, doi:10.1016/j.chemgeo.2005.11.005.

Proskurowski, G., M. D. Lilley, J. S. Seewald, G. L. Früh-Green, E. J. Olson, J. E. Lupton, S. P. Sylva, and D. S. Kelley (2008), Abiogenic hydrocar-bon production at lost city hydrothermal field, *Science*, *319*, 604–607, doi:10.1126/science.1151194.

Reston, T. J., W. Weinrebe, I. Grevemeyer, E. R. Flueh, N. C. Mitchell, L. Kirstein, C. Kopp, and H. Kopp (2002), A rifted inside corner massif on the Mid-Atlantic Ridge at 5°S, *Earth Planet. Sci. Lett.*, *200*, 255–269, doi:10.1016/S0012-821X(02)00636-2.

Roberts, J. J., B. D. Best, D. C. Dunn, E. A. Treml, and P. N. Halpin (2010), Marine geospatial ecology tools: An integrated framework for ecological geoprocessing with ArcGIS, Python, R, MATLAB, and C++, *Environ. Modell. Software*, *25*(10), 1197–1207, doi:10.1016/j.envsoft.2010.03.029.

Ryan, W. B. F., et al. (2009), Global multi-resolution topography synthesis, *Geochem. Geophys. Geosyst.*, *10*, Q03014, doi:10.1029/2008GC002332.

Schmidt, K., A. Koschinsky, D. Garbe-Schonberg, L. M. de Carvalho, and R. Seifert (2007), Geochemistry of hydrothermal fluids from the ultramafic-hosted Logatchev hydrothermal field, 15°N on the Mid-Atlantic Ridge: Temporal and spatial investigation, *Chem. Geol.*, *242*, 1–21.

Schrenk, M. O., D. S. Kelley, J. R. Delaney, and J. A. Baross (2003), Incidence and diversity of microorganisms within the walls of an active deep-sea sulfide chimney, *Appl. Environ. Microbiol.*, *69*(6), 3580–3592, doi:10.1128/AEM.69.6.3580-3592.2003.

Schrenk, M. O., B. J. Brazelton, N. Carolina, and S. Q. Lang (2013), Serpentinization, carbon, and deep life, *Rev. Mineral.*, *75*, 575–606, doi:10.2138/rmg.2013.75.18.

Schroeder, T., and B. E. John (2004), Strain localization on an oceanic detachment fault system, Atlantis Massif, 30°N, Mid-Atlantic Ridge, *Geochem. Geophys. Geosyst.*, *5*, Q0AG11, doi:10.1029/2004GC000728.

Schroeder, T., B. John, and B. R. Frost (2002), Geologic implicationsvof seawater circulation through peridotite exposed at slowspreading\r-mid-ocean ridges, *Geology*, *30*(4), 367–370.

Schulte, M., D. Blake, T. Hoehler, and T. McCollom (2006), Serpentinization and its implications for life on the early earth and mars, *Astrobiology*, *6*(2), 364–376.

Searle, R. C., M. Cannat, K. Fujioka, C. Mével, H. Fujimoto, A. Bralee, and L. Parson (2003), FUJI dome: A large detachment fault near 64°E on the very slow-spreading southwest Indian Ridge, *Geochem. Geophys. Geosyst.*, *4*(8), 9105, doi:10.1029/2003GC000519.

Seyfried, W. E., N. J. Pester, K. Ding, and M. Rough (2011), Vent fluid chemistry of the Rainbow hydrothermal system (36°N, MAR): Phase equilibria and in situ pH controls on subseafloor alteration processes, *Geochim. Cosmochim. Acta*, *75*, 1574–1593.

Smith, D. K., J. R. Cann, and J. Escartín (2006), Widespread active detachment faulting and core complex formation near 13 degrees N on the Mid-Atlantic Ridge, *Nature*, *442*, 440–443, doi:10.1038/nature04950.

Smith, D. K., J. Escartín, H. Schouten, and J. R. Cann (2008), Fault rotation and core complex formation: Significant processes in seafloor formation at slow-spreading mid-ocean ridges (Mid-Atlantic Ridge, 13°-15°N), *Geochem. Geophys. Geosyst.*, *9*, Q03003, doi:10.1029/2007GC001699.

Tucholke, B. E., J. Lin, and M. C. Kleinrock (1998), Megamullions and mullion structure defining oceanic metamorphic core complexes on the Mid-Atlantic Ridge, *J. Geophys. Res.*, *103*, 9857–9866, doi:10.1029/98JB00167.